EXERGY ANALYSIS AND REFRIGERANT EFFECT ON THE OPERATION AND PERFORMANCE LIMITS OF A ONE STAGE VAPOR COMPRESSION REFRIGERATION SYSTEM

Camelia STANCIU, Adina GHEORGHIAN, Dorin STANCIU, Alexandru DOBROVICESCU

POLITEHNICA UNIVERSITY OF BUCHAREST, Romania.

Rezumat. Lucrarea prezinta o analiza comparativa a efectului agentului frigorific utilizat asupra functionarii si performantelor unei instalatii frigorifice cu comprimare mecanica de vapori intr-o treapta. Parametrii si factorii ce influenteaza performantele (din punct de vedere al puterii frigorifice, coeficientului de performanta, consumului de energie, etc) sunt estimate pe baza analizei exergetice. Diverse studii de sensibilitate sunt prezentate comparativ pentru cativa agenti frigorifici (R22, R134a, R717, R507a, R404a). Sunt prezentate rezultate grafice si numerice. Influenta raportului de comprimare este evidentiata pentru functionarea sistemului cu acesti agenti frigorifici, afectand regimul de functionare (temperatura maxima acceptata), respectiv performantele sistemului. De asemenea, se studiaza efectul subracirii si supraincalzirii. In concluzie, se prezinta o analiza comparativa a coeficientului de performanta definit pe baza energetica si a randamentului exergetic.
Cuvinte cheie: comprimare mecanica, instalatie frigorifica, analiza exergetica, subracire si supraincalzire, efectul agentului frigorific.

Abstract. This paper deals with a comparative analysis of the refrigerant impact on the operation and performances of a one stage vapor compression refrigeration system. Parameters and factors affecting the performances (in terms of refrigeration power, coefficient of performance, mechanical work consumption, etc) are evaluated on the basis of an exergy analysis. Different sensitivity studies are presented in a comparative manner for some refrigerants (R22, R134a, R717, R507a, R404a). Graphical and numerical results are included. The effect of compression ratio is emphasized for the system operation working with these refrigerants, affecting the operation regime (maximum accepted temperature), respectively the performances of the system. Also the effects of subcooling and superheating are shown. As conclusion, a comparative analysis between energetic base COP and exergetic efficiency is presented.
Keywords: vapor compression, refrigeration system, exergy analysis, subcooling and superheating, refrigerant impact.

1. INTRODUCTION

This paper deals with a comparative analysis of the refrigerant impact on the operation and performances of a one stage vapor compression refrigeration system. The authors have chosen this type of system, the simplest one, since the aim of the paper is to present and propose an analysis model for comparing the operation of a VCR System with different refigerants, from performances point of view and from limitations in terms of compression ratio. As stated above, the aim is to undersand the mathematical procedure and not to focus on a complex system for the numerical application.

It is well known the fact that after 90's CFC and HCFC refrigerants have been forbiden due to clorine content and their high ozone depleting potential (ODP) and global warming potential (GWP). Thus, HFC refrigerants are used nowadays, presenting a much lower GWP value, but still high with respect to non-flourine refrigerants.

Many research papers have been published on this subject, of replacing "old" refrigerants with "new" ones [1-6]. Lately, many papers focused on researches about finding better and better refrigerants or mixtures, considering different criteria, as for example: ODP and GWP values, performances (COP, TEWI analysis, refrigerating power, compressor consumption, exergetic efficiency), flammability, mass flow rates limitations for safety operation, miscibility with oil, etc [1,3]. Also exergetic analyses and thermoeconomic optimization procedures have been published in the field [7-9].

This paper presents a comparative analysis of five refrigerants working in a one stage VCRS with subcooling and superheating. These five refrigerants are: 1,1,1,2-tetrafluoroethane (HFC-134a), chlorodifluoromethane (R22), ammonia (R717), a near-azeotropic blend (R404a) and an azeotropic blend (R507a). R507a is an azeotropic blend of pentafluorethane R125 and 1,1,1-trifluoroethane R143a with mass percentages of 50% / 50%. R404a is a near-azeotropic blend of R125 / R143a / R134a with mass percentages of 44% / 52% / 4%. Blends do not necessarily remain at constant temperature during constant pressure evaporation or condensation. R134a has the advantage of presenting zero ODP, but still a quite high value for GWP (1300 times higher that that of CO_2), being a chosen substitute for the "old" R12. Spauschus [2] presented the compressor and refrigerant system requirements for substituting R12 with R134a. Havelsky [6] also studied this replacement and others, as R22, R401a, etc. Experimental results on simple VCRS [1,5] have also been presented regarding the behavior of the system working with different refrigerants or mixtures.

We will focus our attention on the operating limits in terms of compression ratio, on system performances when wotking with different refrigerants and on exergy destruction rates in each component of the system to compare the effect of the refrigerants on the system operation.

2. SYSTEM DESCRIPTION

A one stage vapor compression refrigeration system is considered as numerical exemplification of the proposed study. The system is composed by a mechanical piston compressor, a condenser, a throttling valve and an evaporator, as shown in Figure 1. An usual operating cycle, with superheating and subcooling, is represented in p-h coordinates in Figure 2.

The refrigerant enters the compressor at state 1, with a superheating degree ΔT_{SH} with respect to the evaporation temperature T_V. It follows the irreversible compression process 1-2, characterized by an increase in entropy from state 2s (adiabatic reversible compression) to state 2. The refrigerant leaves the compressor as superheated vapor at pressure p_C and enters the condenser and subcooler, arriving in state 3 as subcooled liquid, that is further throttled during the process 3-4. Its pressure is the vaporization pressure p_V and the cycle is closed by a vaporization process 4-1 in the evaporator and superheater.

The simplicity of the system allows the reader to focus on the mathematical model, rather than on its operation.

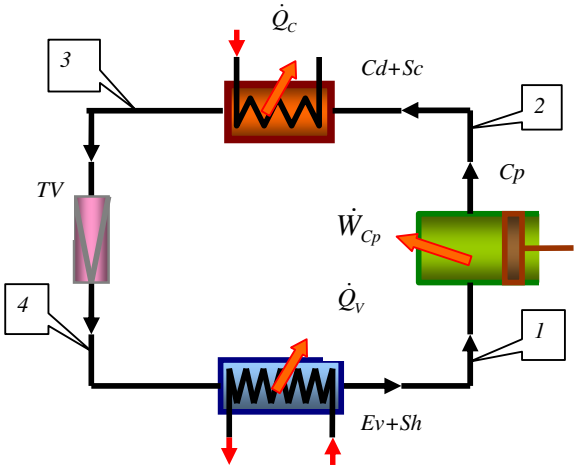

Fig. 1. One stage VCRS

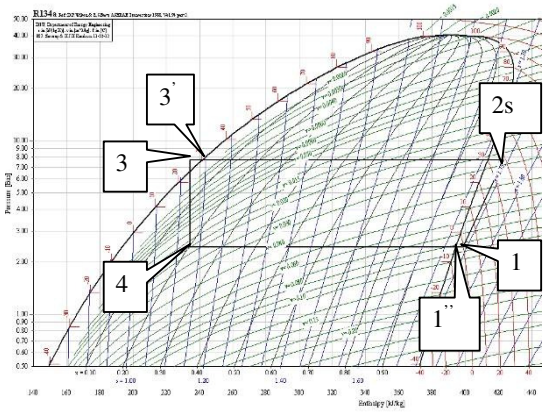

Fig. 2. Usual operating cycle, with superheating and subcooling (p-h coordinates)

3. MATHEMATICAL MODEL

The system is analyzed both from energetic and exergetic points of view. The reader should notice that the two approaches form a more powerful tool in the study and optimization of such systems and one does not exclude the other.

3.1. Energetic approach

This analysis is applied either to each device (seen as a control volume) or to the entire system (a control mass).

It is based on the First Law of Thermodynamics, whose mathematical expression for a control volume is:

$$\frac{dE_{CV}}{d\tau} = \sum_i \left(h + \frac{w^2}{2} + gz\right)_i \dot{m}_i - \sum_o \left(h + \frac{w^2}{2} + gz\right)_o \dot{m}_o + \dot{Q}_{CV} - \dot{W}_{CV} \quad (1)$$

where E represents system energy [J], τ stands for time [s], h is the specific enthalpy of

refrigerant[J/kg], $w^2/2$ is the specific kinetic energy [J/kg], gz is the specific potential energy [J/kg], $\dot{m}$ is the mass flow rate of refrigerant [kg/s], $\dot{Q}$ and $\dot{W}$ [W] are the energetic exchanges of the control volume with its surroundings in form of heat flux and work rate (power).

The subscripts *i* and *o* stands for inlet and outlet states, respectively.

For steady state operation, eq.(1) becomes:

$$\dot{Q}_{CV} = \sum_o \left(h + \frac{w^2}{2} + gz \right)_o \dot{m}_o - \sum_i \left(h + \frac{w^2}{2} + gz \right)_i \dot{m}_i + \dot{W}_{CV} \quad (2)$$

Neglecting the variation of kinetic and potential energies (which is an appropriate assumption in a VCRS), equation (2) becomes:

$$\dot{Q}_{CV} - \dot{W}_{CV} = \sum_o (\dot{m}h)_o - \sum_i (\dot{m}h)_i \quad (3)$$

which is applied to each device of the system:

a) for the evaporator (phase change process in a heat exchanger):

$$\dot{Q}_V = \dot{m}(h_1 - h_4) \quad (4)$$

where $\dot{Q}_V$ [W] represents the refrigerating load, while the specific enthalpy h is determined by using the Engineering Equation Solver (EES) software;

b) for the condenser (phase change process in a heat exchanger):

$$\dot{Q}_C = \dot{m}(h_3 - h_2) \quad (5)$$

where $\dot{Q}_C$ [W]is the condenser thermal load;

c) for the compressor (compression process):

$$\dot{W}_{Cp} = \dot{m}(h_1 - h_2) + \dot{Q}_{Cp} \quad (6)$$

where $\dot{Q}_{Cp}$ is the heat rate generated in a non – adiabatic compressor, estimated as:

$$\dot{Q}_{Cp} = \dot{m}(h_2 - h_{2s}) \quad (6')$$

d) for the throttling valve (throttle process, isenthalpic):

$$\dot{m}h_3 = \dot{m}h_4 \quad (7)$$

The sign convention is the English one, namely all heat rejected by the system is negative and all heat received by the system is positive; the consumed mechanical work is negative.

The energetic efficiency of the system is measured by the coefficient of performance:

$$COP = \frac{usefull\ effect}{consumption} = \frac{\dot{Q}_V}{|\dot{W}_{Cp}|} \quad (8)$$

By applying the Second Law of Thermodynamics to each control volume, one could find the entropy generation in the system:

$$\dot{S}_{gen} = \frac{dS_{CV}}{d\tau} + \sum_o (\dot{m}s)_o - \sum_i (\dot{m}s)_i - \sum_j \left(\frac{\dot{Q}_j}{T_j} \right)_{ext} \quad (9)$$

where $dS_{CV}/d\tau$ is zero for a steady state operation regime; $\dot{Q}_j/T_j$ represents the heat flux $\dot{Q}_j$ exchanged by the system with the surroundings at T_j temperature level and *s* [J/(kgK)] represents the specific entropy of the refrigerant.

By applying Eq. (9) to each device of the system, one gets:

a) for the evaporator:

$$\dot{S}_{gen,V} = \dot{m}(s_1 - s_4) - \frac{\dot{Q}_V}{T_V} \quad (10)$$

where T_V [K] is the vaporization temperature;

b) for the condenser:

$$\dot{S}_{gen,C} = \dot{m}(s_3 - s_2) + \frac{|\dot{Q}_C|}{T_0} \quad (11)$$

c) for the compressor:

$$\dot{S}_{gen,Cp} = \dot{m}(s_2 - s_1) + \frac{|\dot{Q}_{Cp}|}{T_0} \quad (12)$$

d) for the throttling valve:

$$\dot{S}_{gen,TV} = \dot{m}(s_4 - s_3) \quad (13)$$

The specific entropy *s* [J/kgK] is determined for each state of the refrigerant by using the EES software.

In Table 1, one can notice how these state parameters of the refrigerant are determined in each state during the operating cycle.

Table 1
Determination of state parameters

State	Independent parameters	Specific parameters
1"	p_V , $x_{1"} = 1$	$h_{1"}$, $s_{1"}$, $v_{1"}$
1	p_V , $t_1 = t_V + \Delta t_{SH}$	h_1 , s_1 , v_1
2*s*	p_C , $s_{2s} = s_1$	h_{2s} , s_{2s} , v_{2s}
2	p_C , h_2	h_2 , s_2 , v_2
3'	p_C , $x_{3'} = 0$	$h_{3'}$, $s_{3'}$, $v_{3'}$
3	p_C , $t_3 = t_C - \Delta t_{SC}$	h_3 , s_3 , v_3
4	p_V , $h_4 = h_3$	h_4 , s_4 , v_4

where $h[J/kg]$, $s[J/kgK]$, $v[m^3/kg]$.

The enthalpy of the real state 2 is determined by introducing the compressor adiabatic efficiency, namely: $h_2 = h_1 + \frac{\eta_{Cp}}{h_{2s} - h_1}$, where the adiabatic

efficiency is estimated by using an empirical relation: $\eta_{Cp} \approx 1 - 0.05\frac{p_C}{p_V}$ [10].

By concluding this approach, all specific properties are determined in all states of the cycle, and also all energetic exchanges of the system with its surroundings are computed.

3.2. Exergetic approach

The exergetic balance equation for a control volume is:

$$\frac{dEx_{CV}}{d\tau} = \sum_j \dot{E}x_{Q_j} - \left(\sum \dot{W} - p_0\frac{dV}{d\tau}\right) + \sum_i (\dot{m}ex)_{-_i} - \sum_o (\dot{m}ex)_o - \sum I \quad (14)$$

where $\dot{I}$ [W] represents the exergy distruction rate, ex [J/kg] represents the specific exergy of the refrigerant, $\dot{E}x_{Q_j}$ [W] is the heat exergy rate.

For steady state operation, Eq. (14) becomes:

$$\sum \dot{I} = \sum_i (\dot{m}ex)_i - \sum_o (\dot{m}ex)_o + \sum_j \dot{E}x_{Q_j} - \sum \dot{W} \quad (15)$$

The specific exergy of the refrigerant is computed as:

$$ex = (h - h_0) - T_0(s - s_0) \quad (16)$$

The heat exergy rate $\dot{E}x_Q$ in Eq. (15) is expressed as:

$$\dot{E}x_Q = \dot{Q}\left(1 - \frac{T_0}{T_{boundary}}\right) \quad (17)$$

In Eq. (16) and (17), the subscript "*0*" denotes the extensive parameters of the system brought in the restrictive dead state.

The standard parameters of the environment are: $T_0 = 299{,}15K$, $p_0 = 1bar$.

According to Guy – Stodola theorem, the exergy distruction rate is also computed by:

$$\dot{I} = T_0\dot{S}_{gen}. \quad (18)$$

or can be determined by applying Eq. (15) to each component of the system:

a) for the evaporator:

$$\dot{I}_V = \dot{m}ex_4 - \dot{m}ex_1 + \dot{Q}_V\left(1 - \frac{T_0}{T_V}\right) \quad (19)$$

By replacing Eq. (16) in (19) and neglecting the variation of kinetic and potential energies, one gets:

$$\dot{I}_V = \dot{m}[(h_4 - T_0s_4) - (h_1 - T_0s_1)] + \dot{Q}_V\left(1 - \frac{T_0}{T_V}\right) \quad (20)$$

By applying the same reasoning, one gets:

b) for the condenser:

$$\dot{I}_C = \dot{m}ex_2 - \dot{m}ex_3 = \\ = \dot{m}[(h_2 - T_0s_2) - (h_3 - T_0s_3)] \quad (21)$$

c) for the compressor:

$$\dot{I}_{Cp} = \dot{m}ex_1 - \dot{m}ex_2 + |\dot{W}_{Cp}| = \\ = \dot{m}[(h_1 - T_0s_1) - (h_2 - T_0s_2)] + |\dot{W}_{Cp}| \quad (22)$$

d) for the throttling valve:

$$\dot{I}_{TV} = \dot{m}ex_3 - \dot{m}ex_4 = \dot{m}[(h_3 - T_0s_3) - (h_4 - T_0s_4)] = \\ = \dot{m}T_0(s_4 - s_3) \quad (23)$$

The overall exergy distribution rate is:

$$\dot{I}_{TOT} = \dot{I}_V + \dot{I}_C + \dot{I}_{Cp} + \dot{I}_{TV} \quad (24)$$

The exergetic efficiency of the system is evaluated:

$$\eta_{ex} = \frac{\dot{E}x_P}{\dot{E}x_F} \quad (25)$$

where the product exergy rate is:

$$\dot{E}x_P = \dot{Q}_V\left(1 - \frac{T_0}{T_V}\right) \quad (26)$$

and the fuel exergy rate is:

$$\dot{E}x_F = |\dot{W}_{Cp}| \quad (27)$$

The exergy balance equation applied to the whole system gives:

$$\dot{E}x_F = \dot{E}x_P + \dot{I}_{TOT} \quad (28)$$

By combining Eq. (26) – (29), one gets:

$$\eta_{ex} = 1 - \frac{\dot{I}_{TOT}}{\dot{E}x_F} = \frac{\dot{Q}_V}{|\dot{W}_{Cp}|}\left(1 - \frac{T_0}{T_V}\right) \quad (29)$$

Remembering Eq. (8) and the expression of *COP* for an inverse Carnot cycle working between T_0 and T_V temperature levels, one obtains:

$$\eta_{ex} = \frac{COP}{COP_{CC}\big|_{T_V}^{T_0}} \quad (30)$$

This exergetic efficiency measures the system behavior with respect to a corresponding Carnot cycle working between the same vaporization temperature and the surroundings one. Thus, it measures the irreversibilities of the real operation with respect to a theoretical possible operation.

Graphical results are presented for these system performances, in a comparative manner for the studied refrigerants and for different sets of parameters values in some sensitivity studies.

4. RESULTS

In order to make a comparison of the refrigerant effect on the operation of the VCRS, the compression ratio, β, is varied between 2 and 16. The first check is on the refrigerant temperature at the compressor outlet, t_2, represented in Figure 3.

One may suppose that the maximum allowed limit of operation is 140°C for this temperature, due to compressor oil inflammability limit. Thus, in this figure one could compare the maximum allowed compression ratio for the studied refrigerants. The ammonia (R717) has the lower limit in terms of β, as known. It is also interesting to notice the fact that R134a, which replaced R22 in domestic refrigerators, has a higher limit than the last one. The two near (azeotropic) mixtures are very close in terms of maximum compression ratio, as it was expected.

The corresponding vaporization temperatures are shown in Figure 4, where the dotted flashes represent the values corresponding to maximum compression ratio. One can notice that the system operating at a compression ratio of 5 could achieve a vaporization temperature of -10°C when operating with ammonia (R717), -15°C for R22 and 0°C for R134a. Also, when operating at the

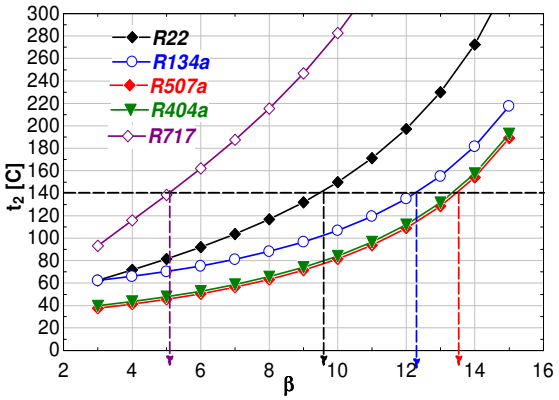

Fig. 3. Refrigerant effect on the maximum allowed compression ratio

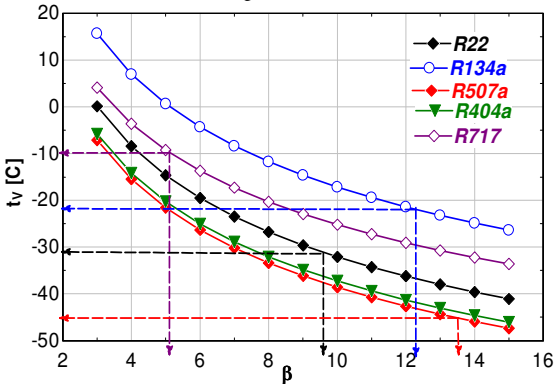

Fig. 4. Refrigerant indirect effect on the maximum attainable vaporization temperature

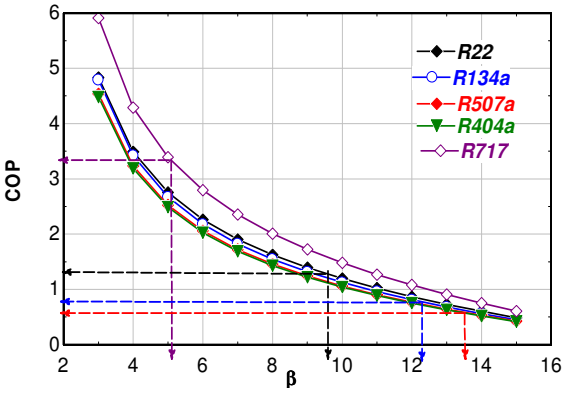

Fig. 5. Refrigerant indirect effect on the maximum attainable COP

maximum allowed value of β, R134a could lead to a possible minimum value of -20°C with respect to -30°C for R22 and -45 for the azeotropic mixtures. Ammonia (R717) is restricted to -10°C.

The comparison in terms of operation performances could be studied in Figures 5 (coefficient of performance), Figure 6 (exergetic efficiency), Figure 7 (inlet volume flow rate) and Figure 8 (specific refrigerating power). As it is known, R717 presents the highest refrigerating power, for intake volume flow rate close to the values of the other studied refrigerants.

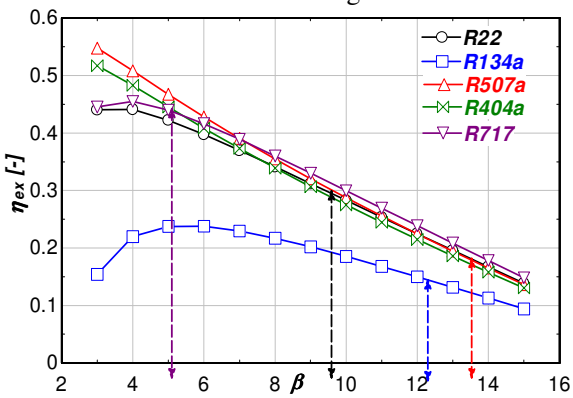

Fig. 6. Refrigerant indirect effect on the maximum attainable exergetic efficiency

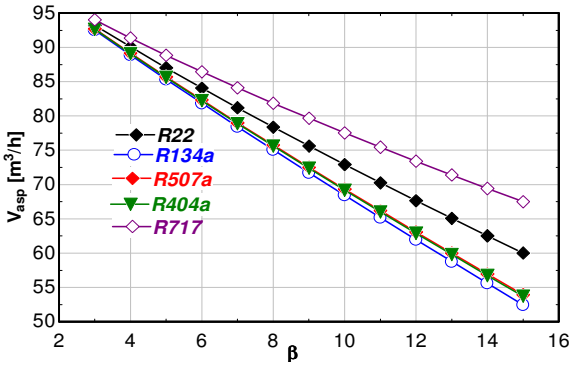

Fig. 7. Refrigerant volume rate at compressor inlet

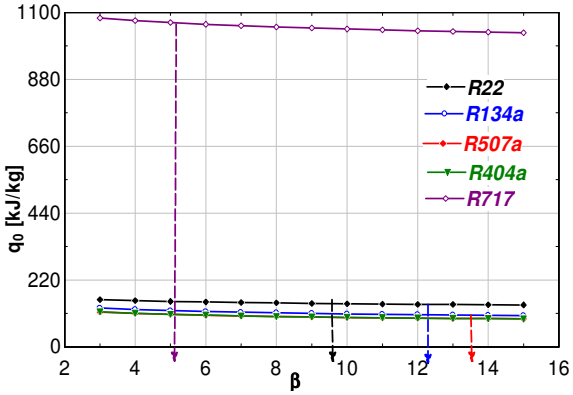

Fig. 8. Refrigerant indirect effect on the maximum attainable specific refrigerating load

In Figures 9-11 one could notice the effect of superheating on the maximum allowed compression ratio and in terms of coefficient of performance. As one might expect, a superheating degree (here of 10°C) increased the outlet temperature of the refrigerant reducing the maximum value of β and

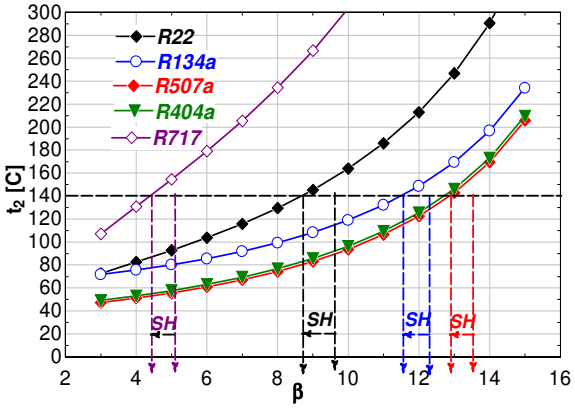

Fig.9. Refrigerant effect on the maximum allowed compression ratio, with 10°C of superheating; comparison to the case of no superheating

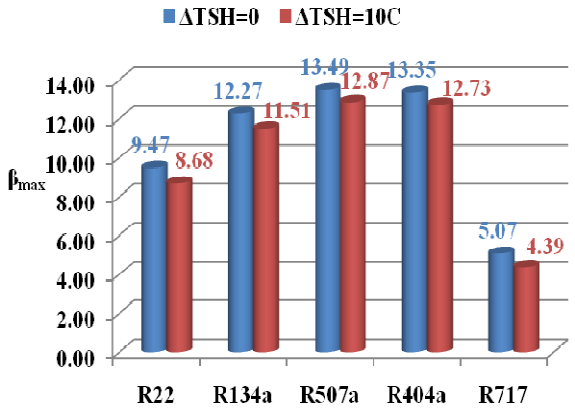

Fig. 10. Comparison between maximum allowed compression ratio, influence of superheating

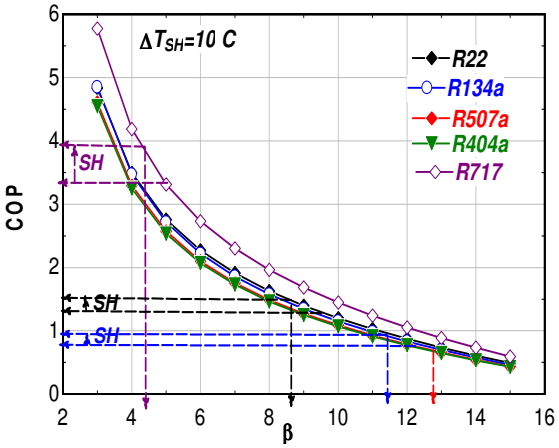

Fig. 11. Refrigerant effect on the maximum attainable COP, with 10°C of superheating; comparison to the case of no superheating

increasing the coefficient of performance. The most important effect on *COP* of superheating is presented by R717.

Regarding irreversibilities during VCRS operation, in Figure 12 one may see the repartition of exergy destruction rates on each component of the system (C-condenser, Cp-compressor, TV-throttling valve, V-evaporator) for the five refrigerants. One can notice that ammonia presents the highest values. It is also interesting to notice that the highest exergy destruction rate is in the compressor for R134a, R717 and almost for R22,

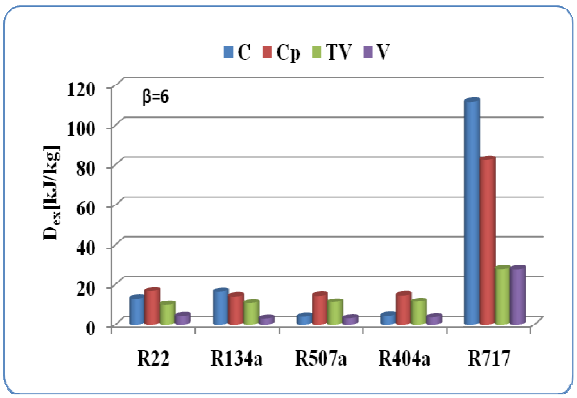

Fig. 12. Refrigerant effect on the exergy destruction rates in the condenser (C), compressor (Cp), throttling valve (TV) and evaporator (V), no superheating and β=6

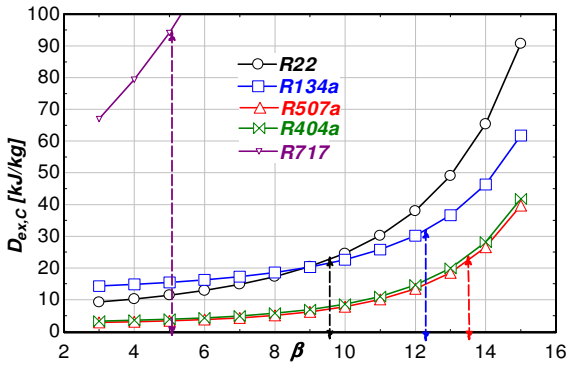

Fig. 13. Refrigerant effect on the exergy destruction rates in the condenser, no superheating

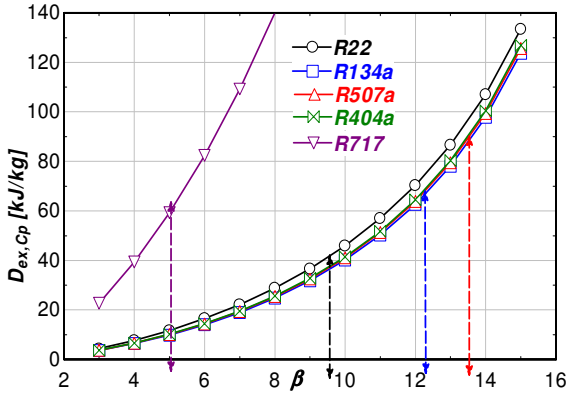

Fig. 14. Refrigerant effect on the exergy destruction rates in the compressor, no superheating

while the two azeotropic blends leads to a higher exergy destruction rate in the compressor, although in the studied numerical example, the temperature variation during phase change process is about 0.4°C. The lower values of the exergy destruction rates in the condenser are due to the lower values of the condensation temperature and thus the temperature gap between the refrigerant and the environnement during this phase change process. This information could be used when optimizing the system, in temrs of the component that should be focused, depending thus on the refrigerant.

Figures 13 and 14 show the variation of exergy destruction rates in condenser (Figure 13) and compressor (Figure 14) with the compression ratio and working refrigerant. Higher the compression ratio is, higher the destruction rates are. The differences when comparing the refrigerants are mostly due to condenser destruction rates. Ammonia has a special behavior, as the exergy destruction rate is very sensitive to β. Studying the behavior of the vapor compression refrigerating system in different conditions could bring important information about the components that should be optimized and about the most suitable refrigerant (among available alternatives).

5. CONCLUSIONS

A comparative analysis of the refrigerant impact on the operation and performances of a one stage vapor compression refrigeration system was presented. The effects of compression ratio and superheating were studied on the system operation and performances. Based on the exergy analysis, exergy destruction rates were estimated for each component of the system in a comparative manner for five refrigerants (R22, R134a, R717, R507a, R404a) proving a different behavior and thus bringing important information about system optimization when working with a specific refrigerant.

Aknowledgements

This work was supported by CNCSIS-UEFISCU, project number PNII – IDEI – 1719/2009.

REFERENCES

[1] M. Padilla, R. Revellin, J. Bonjour – *Exergy analysis of R413A as replacement of R12 in a domestic refrigeration system*. Energy Conversion and Management 51, 2195–2201 (2010).

[2] H.O.Spauschus - *HFC 134a as a substitute refrigerant for CFC 12.* . Int J Refrig 11:389–92 (1988).

[3] J.U. Ahamed, R.Saidur, H.H.Masjuki - *A review on exergy analysis of vapor compression refrigeration system*. Renewable andSustainableEnergyReviews 15, 1593–1600 (2011).

[4] R. Llopis, E. Torrella, R. Cabello, D. Sánchez - *Performance evaluation of R404A and R507A refrigerant mixtures in an experimental double-stage vapour compression plant*. Applied Energy 87, 1546–1553 (2010).

[5] A. Aroraa, S.C. Kaushik - *Theoretical analysis of a vapour compression refrigeration system with R502, R404A and R507A*. International Journal of Refrigeration 31, 998 – 1005 (2008).

[6] V. Havelsky´ - *Investigation of refrigerating system with R12 refrigerant replacements*. Appl Therm Eng;20:133–40 (2000).

[7] T. Morosuk, G. Tsatsaronis – *Advanced exergetic evaluation of refrigeration machines using different working fluids*. Energy 34, 2248 ‑ 2258 (2009).

[8] R. Selbas, O. Kı zı lkan, A. Sencan - *Thermoeconomic optimization of subcooled and superheated vapor compression refrigeration cycle*. Energy 31, 2108 ‑ 2128 (2006).

[9] R. Yumrutas, M. Kunduz, M. Kanoglu - *Exergy analysis of vapor compression refrigeration systems*. Exergy, an International Journal 2, 266–272 (2002).

[10] J. Desmons – *Aide-memoire Froid industriel*. DUNOD (2010).

[11] A. Dobrovicescu - *Analiza exergetica si termoeconomica a sistemelor frigorifice si criogenice*. AGIR (2000).

[12] A. Dobrovicescu – „*De ce Exergie? De ce Exergoeconomie?*”. Volumul colocviului Colloque Franco-Roumain Energy, Environment, Economie et Thermodynamique – COFRET, Bucureşti (2002).

THEORETICAL AND EXPERIMENTAL STUDY ON CRYOGENIC FREEZING OF RASPBERRIES AND BLUEBERRIES

Valeriu DAMIAN[1], Cristian IOSIFESCU[1], Thi Hoa NGUYEN[2]

[1]UNIVERSITY "DUNAREA DE JOS", Galati, Romania.
[2]UNIVERSITY OF TRANSPORT AND COMMUNICATIONS, Hanoi, Vietnam.

Rezumat. Lucrarea prezintă aspecte legate de congelarea criogenică cu azot lichid a fructelor de pădure (zmeură şi afine): durata procesului, capacitatea de congelare, avantajele şi dezavantajele metodei. Congelarea rapidă constă în folosirea într-un congelator criogenic atât a căldurii latente de vaporizare a azotului lichid, cât şi a căldurii specifice a vaporilor de azot formaţi, a căror temperatură creşte până la temperatura finală a produsului congelat. Metoda foloseşte pentru congelare azot lichid, care are avantajul costului redus, fiind obţinut ca produs secundar în urma procesului de separare a aerului.
Cuvinte cheie: congelare criogenică, fructe de pădure, conservarea alimentelor.

Abstract. This paper presents some aspects concerning raspberries and blueberries freezing using liquid nitrogen: duration of the process, freezing capacity, advantages and disadvantages of this modern method. Quick freezing of food products in a cryogenic freezer consist in the use latent heat of evaporation of the liquid nitrogen, as well as of the sensible heat of the vapors, whose temperature increase up to final temperature of the frozen product. The use of cryogenic freezing with liquid nitrogen and carbon-dioxide is regarded as the "century's revolution" in the food area. Considering the demands for reduction of fuel consumption involved in generation of electrical energy needed for classical refrigeration systems, this method uses for freezing liquid nitrogen obtained as secondary product at oxygen production.
Keywords: freezing, nitrogen, cryogenic, food preservation, raspberries, blueberries.

1. INTRODUCTION

Freezing is the favorite modern mean for best preservation of nutrient and organoleptical properties of a large number of alimentary products, ensuring long term preservation. Direct contact freezing using liquids (nitrogen or CO_2), is done either by sinking the product in a cold liquid or by spraying the product with this liquid. The liquid can evaporate or not, but in either cases, the method has the main advantage of a great improvement of the heat transfer coefficient between the product to be frozen and the refrigerant.

Using cryogenic systems one can avoid the large investment required for a compression refrigeration system, using only from time to time cold delivery in the shape of the liquefied cryogenic fluid.

2. REQUIRED FREEZING TIME

Freezing is the process by which most of the water from the cellular liquid and the water from a product's tissues (capillary vases, intercellular spaces) is turned into ice. Water crystallization temperature ranges between -1…-5 ^{o}C, at which 60…75 % of the whole water content turns into solid.

The process must be continued afterwards by subcooling the product to a final temperature of -18…-25 ^{o}C, at which 90…95 % of the water content turns into solid. Thermal core temperature is a main indicator of the end of the freezing process as it can be with maximum 3…5 ^{o}C higher than the products' storage temperature.

International Institute of Refrigeration established the following conditions: final temperature of the products thermal core ≤ -15 ºC, average final temperature ≤ -18 ºC. Freezing process of a food product is a typically transient heat and mass transfer process.

Transfer phenomenon is complex due to the phase change of the solidifying water and of the transport properties of the product (thermal conductivity, specific heat, etc.).

Computing methods use some simplifying assumptions which allow establishing some simple calculus relations for the freezing duration (according to Plank):

- all the heat is drawn from the product at the freezing point temperature,
- the products are homogenous and isotropic,
- the cooling surroundings has a constant temperature,
- the product has already been cooled down to the freezing temperature.

Total duration of the freezing process is:

$$\tau_c = \tau_r + \tau_{cg} + \tau_{sr} \quad [\text{s}] \tag{1}$$

where: τ_r [s] - primary refrigeration duration; τ_{cg} [s] - freezing duration; τ_{sr} [s] - product duration subcooling;

Primary refrigeration duration can be computed from the following relation:

$$\tau_r = \frac{m \cdot c}{\alpha \cdot s} \cdot \ln \frac{t_i - t_{mI}}{t_f - t_{mI}} \quad [\text{s}] \tag{2}$$

$$m = \rho \cdot V \ [\text{kg}] \tag{3}$$

$$V = \frac{4 \cdot \pi \cdot r_0^3}{3} \quad [\text{m}^3] \tag{4}$$

Where: m - product mass; ρ - density; c - specific heat; α - convection coefficient; s - product's external area; t_I - initial temperature; t_f - final temperature; t_{mI} - cooling surrounding temperature (zone I);

For a spherical shape product, freezing duration can be determined using Plank's formula [4]:

$$\tau_{cg} = \frac{\rho \cdot l_{cg}}{t_{cg} - t_{mII}} \cdot \left(\frac{r_0^2}{6 \cdot \lambda} + \frac{r_0}{3 \cdot \alpha} \right) \tag{5}$$

where: t_{cg} - freezing temperature; t_{mII} - cooling surrounding temperature (zone II); α - convection coefficient; r_0 - sphere radius; l_{cg} - freezing latent heat; ρ - density; λ - thermal conductivity;

The duration for subcooling of the frozen product to the final average temperature (t_{mf}) can be calculated using Plank's relation:

$$\tau_{sr} = 933 \cdot c_m \cdot n \cdot \left| \lg \frac{t_{cg} - t_{mIII}}{t_{III} - t_{mII}} - 0{,}0913 \right| \cdot \left(\frac{2 \cdot r_0}{\alpha} + \frac{r_0^2}{\lambda} \right) \cdot \frac{1}{3{,}6}$$

[h] (6)

where:

t_{cg} - freezing final temperature;

t_{mII} - cooling surrounding temperature (zone III);

t_{mIII} - thermal core final temperature of the product;

c_m - frozen product average specific heat;

n - dimensionless coefficient, whose values depends on the Biot dimensionless group, defined by:

$$Bi = \frac{\alpha \cdot \delta}{\lambda} \tag{7}$$

where $\delta = r_0$.

Table 1
Values for the dimensionless coefficient n vs. Bi [4]

Bi	n
0,25	1,21
0,5	1,188
1,0	1,156
2,0	1,112
4,0	1,06
10	1,02
∞	1,00

3. RESULTS AND CONCLUSIONS

The paper analyses the freezing process duration for blueberries and raspberries.

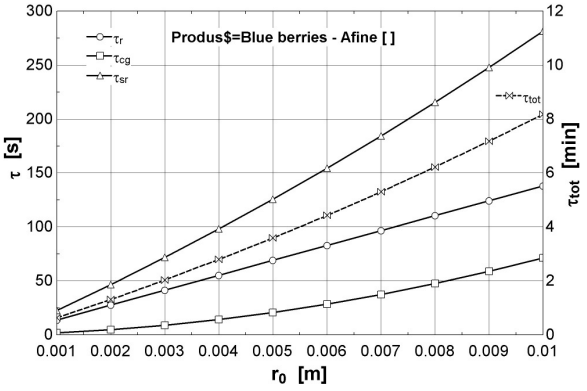

Fig. 1. Influence of product radius on partial and total freezing times

Various properties of the considered products are presented in the Table 2.

The cooling environment average temperatures (t_{mI}, t_{mII}, t_{mIII}) as well as the product temperatures (t_{cg}, t_{mIII}) were measured using digital display thermocouples.

Table 2
Various properties of the considered products

Property\ Product	Blueberries	Raspberries
t_c [C]	-2.6	-1.1

c_{pI} [kJ/kgK]	3770	3520
c_{pIII} [kJ/kgK]	1930	1840
l_{cg} [kJ/kg]	288.4	283.8
u [%]	87.4	82
λ [W/m-K]	0.54	0.49
ρ [kg/m^3]	1000	998

As one can notice in Figure 1, increased size of products radius r_0 in the range of 1 … 10 mm leads, as expected, to increased partial durations, and therefore an increased total duration for the entire freezing process. For the same product size, due to the different properties, blueberries have a slightly longer process time than raspberries (for the reference case with r_0 = 5e-03 m: $\tau_{tot\ blueberries}$ = 3.59 min, and $\tau_{tot\ raspberry}$ = 3.02 min) - see Figure 2.

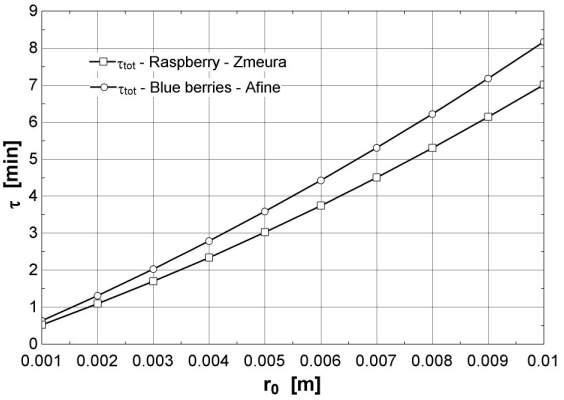

Fig. 2. Total freezing time vs. product radius

Fig. 3 shows the influence on convection coefficients $\alpha_{1,2,3}$ on corresponding process times. As it can be seen, the most powerful influence is the one of the cooling coefficient. Reference values were: α_1 = 35 W/m^2-K, α_2 = 530 W/m^2-K, α_3 = 25 W/m^2-K.

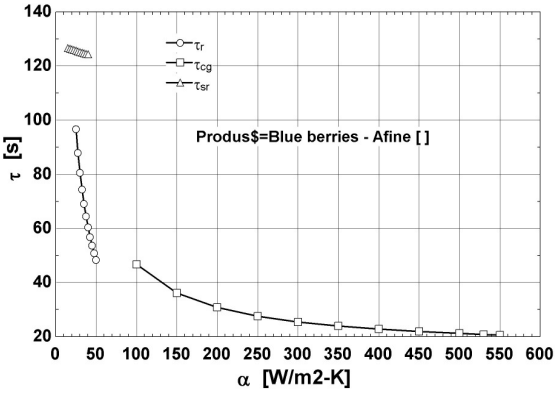

```
ERROR: stackunderflow
OFFENDING COMMAND: ~

STACK:
```

STUDY ON AIR CONDITIONING THROUGH DESICCANT TECHNOLOGY

Carmen Ema PANAITE, Aristotel POPESCU, Bogdan HORBANIUC

GHEORGHE ASACHI TECHNICAL UNIVERSITY, Iasi, Romania.

Rezumat. Lucrarea propune un model matematic pentru studiul proceselor de transfer ce au loc în particula adsorbantă ce intră în componenţa adsorberelor rotative în strat compact. Rezultatele numerice obţinute au permis evidenţierea distribuţiei încărcării solidului adsorbant pe direcţie radială precum şi a variaţiei parametrilor medii ai acestuia (temperatură şi conţinut de umiditate).
Cuvinte cheie: condiţionarea aerului, transfer de căldură şi masă, adsorbţie, modelare.

Abstract. In the present paper, a behavioural model of the transfer processes within the desiccant pellet was proposed. The numerical simulation allowed to obtain the water content distribution on radial direction and the evolution of the average solid desiccant parameters (water content, temperature) during adsoption and desorption stages.
Keywords: air conditioning, heat and mass transfer, desiccant systems, modelling.

1. INTRODUCTION

Due to increasing outdoor temperatures in the last decades, the higher living and working standards and the relatively low prices of air conditioning units, the demand for air conditioning in buildings has sharply risen. This can also be noticed in the anual energy use of room air conditioners which increased from 6 TJ in 1990 to 160 TJ in 2010 [1].

The fast growing demand for air conditioning lead to a significant increase for electricity consumption and thus for primary energy. Electric appliances are used at maximum capacity in the hot summer days, but often fail to meet the demand. The resulting CO_2 emissions in the EU increased twenty times from 1990 to 2010 [1].

Desiccant Evaporative Cooling Systems represent an alternative for the classical methods with mechanical vapor compression [2]. This type of systems can handle sensible and latent heat loads independently without using CFCs or a large amount of electricity. This leads to a high level of comfort, environment protection and less energy used, expanding and promoting desiccant industry from niche applications to a broader market, such as hospitals, supermarkets, restaurants, theatres, schools and office buildings [3]. For small scale systems, there is no market available technology but for development of these systems special research efforts are made.

Desiccant Evaporative Cooling Systems contains three basic components: a rotary adsorber (the dehumidifier) RA, an evaporative cooler EC and a sensible heat exchanger HE.

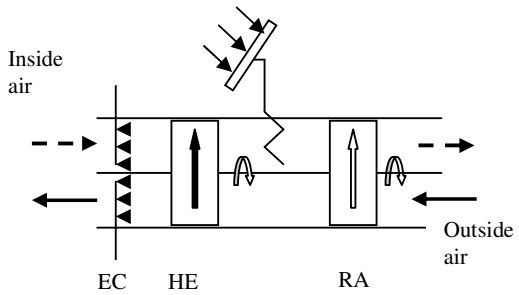

Fig. 1. Basic Desiccant Evaporative Cooling System

The adsorber, of rotary wheel type, is partitioned in two sections that allow flow in opposite directions (Fig. 1). In the process air (outside air) section, the moisture of the air is partially adsorbed by the solid desiccant. The released adsorption heat increases the temperature of the solid and of the air. Therefore, the air exits the process side of the wheel hot and dry. Passing through the sensible heat exchanger of Lungstrom type, most of the added adsorption heat is rejected on the regeneration side where the adsorbent is reactivated.

Nomenclature

c	vapor concentration in air, kg/m^3	x	water content of solid desiccant, kg/kg
c_p	specific heat, J/kgK	x^*	equilibrium water content on the vapor-solid interface, kg/kg
D_M	overall diffusion coefficients, m^2/s	$\overline{x}$	average water content , kg/kg
D_K	Knudsen diffusion coefficient, m^2/s	y	air humidity ratio, kg/kg
D_{12}	gas free diffusion coefficients, m^2/s		
d_p	pore diameter, m		
h	specific enthalpy, J/kg	Greek symbols	
h_B	formation enthalpy, J/kg	ε	porosity of particle
h_c	convection heat transfer coeff., W/m^{2}K	μ_p	tortuosity factor
h_m	mass transfer coefficient, m/s	ρ_s	adsorbent particle density, kg/m^3
h_{lg}	latent heat of vaporization, J/kg	τ	time, sec
h_{lg0}	latent heat of vaporization at 0°C, J/kg		
m	mass, kg	Subscript	
R	radial coordinate, m	b	bulk flow
R_p	pellet radius, m	g	vapor
T	temperature, K	i	initial
w_b	air velocity, m/s	s	solid desiccant

The evaporative process from evaporative cooler reduces substantially the air temperature, while the air humidity is maintained at a proper level.

The improvement of the adsorber performance is the most important step with a view to optimize the whole system. This is the reason why, in the present paper, a theoretical approach started with the heat and mass transfer processes within the desiccant pellet, which is the basic constitutive unit of desiccant wheel, is proposed. Thus, the main elements of some of the actual models were accepted [4] and corrections regarding as the definition and calculus of the adsorption heat and how this involves in the energy balance equation (through formation enthalpy and latent heat of vaporization) were made. Supplementary assumptions were used, such as uniform temperature within the desiccant pellet [5] and the energy storage in both adsorbent and adsorbate phases [6].

2. MATHEMATICAL MODEL

The mathematical model of the heat and mass transfer processes is based on the following main assumptions [4], [6]:

- the desiccant pellet is spherical and its physical properties are uniform;
- the circular macropores are disposed on radial direction, from the surface of the pellet to the central point;
- one adsorption component system is considered (water vapor);
- the heat transfer resistance is concentrated in the external film, thus the internal temperature gradients are low and can be neglected [5];
- the heat of adsorption dependents on water content and temperature of the solid;
- the free gas diffusion and the Knudsen diffusion characterize the mass transfer transport in macropores;
- the vapor diffusion in micropores is insignificantly;
- the equilibrium between gas phase and solid phase is manifested everywhere in the desiccant pellet; the relation between vapor concentration of air and the water content of the solid is expressed by the specific adsorption isotherm $x=x^*=f(c,T)$;
- the heat storage is made in both adsorbent and adsorbate phases.

2.1. Mass balance equation

The mass balance is applied on a control volume that is delimited by two concentrically spherical surfaces of R, respectively R+dR radius (Fig.2).

The control volume contains a fraction of solid desiccant material and a fraction of pores (voids). The macropores are occupied by the adsorbate (water fixed on the internal gas-solid interface) and air with an actual water vapor concentration.

For an elementary period $d\tau$, the mass balance is expressed by the following equations [4], [6]:

$$\left(\dot{m}_{g\,R+dR} - \dot{m}_{g\,R}\right) d\tau = dm_g + dm_a \tag{1}$$

$$\dot{m}_{g\,R+dR} = \dot{m}_{g\,R} + \frac{\partial \dot{m}_{g\,R}}{\partial R} dR \tag{2}$$

The relevant masses for the transport process

are calculated with the following relations:

$$m_g = 4\pi R^2 \cdot dR \cdot \varepsilon \cdot c \tag{3}$$

$$m_g = 4\pi R^2 \cdot dR \cdot \rho_s \cdot x \tag{4}$$

$$\dot{m}_{g\,R} = \frac{D_M}{\mu_P} 4\pi \cdot R^2 \cdot \varepsilon \cdot \frac{\partial c}{\partial R}, \tag{5}$$

where $$D_M = \frac{1}{1/D_{12} + 1/D_K}. \tag{6}$$

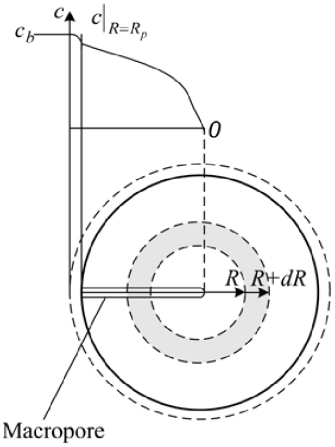

Fig. 2. Control volume for mass balance

Through successive mathematical processing, for the assumptions mentioned above, the final form of the mass balance equation is:

$$\frac{\partial c}{\partial \tau}\left(1 + \frac{\rho_s}{\varepsilon}\frac{\partial x}{\partial c}\bigg|_T\right) + \frac{\rho_s}{\varepsilon}\frac{\partial x}{\partial T}\bigg|_c \frac{\partial T}{\partial \tau} = \frac{D_M}{\mu_P}\left(\frac{\partial^2 c}{\partial R^2} + \frac{2}{R}\frac{\partial c}{\partial R}\right) \tag{7}$$

Energy balance equation

To deduce the energy balance equation, the differential spherical control volume is abandoned. Based on the assumption that the internal temperature gradients are insignificantly, for this analysis stage the entire pellet is considered. The energy stored within the pellet in the elementary period dτ is estimated with the relation:

$$\delta Q_{st} = \left(\dot{Q}_g - \dot{Q}_{cv}\right) \cdot d\tau + \dot{Q}_B \cdot d\tau\,. \tag{8}$$

The following relations were used for the calculus of diffusion heat rate $\dot{Q}_g$, convection heat rate $\dot{Q}_{cv}$ and heat rate corresponding to the formation enthalpy $\dot{Q}_B$:

$$\dot{Q}_g = \frac{D_M}{\mu_P} 4\pi R_p^2 \varepsilon \frac{\partial c}{\partial R}\bigg|_{R=R_p} \left[h_{lg\,0} + c_{pg}\left(T_b - 273{,}15\right)\right] \tag{9}$$

$$\dot{Q}_{cv} = h_c 4\pi R_p^2 \left(T - T_b\right) \tag{10}$$

$$\dot{Q}_B = \frac{\partial \bar{m}_a}{\partial \tau} \cdot h_B = \dot{m}_g\big|_{R=R_p} \cdot h_B\,. \tag{11}$$

The amount of adsorbate, $\bar{m}_a$, which is the average value for the entire pellet, may be expressed as follows:

$$\bar{m}_a = \frac{4}{3}\pi R_p^3 \bar{x} = \int_0^{R_p} 4\pi R^2 \cdot \rho_s \cdot x \cdot dR\,. \tag{12}$$

Using the assumption that the intraparticle heat storage is made in both adsorbent and adsorbate phases, for the calculation of the term δQ_{st} the following equations were used:

$$\begin{aligned}
&\delta Q_{st} = \dot{Q}_{st} d\tau = \frac{\partial}{\partial \tau}\left(\bar{m}_a h_a\right) + \frac{\partial}{\partial \tau}\left(m_s h_s\right) = \\
&= \frac{\partial \bar{m}_a}{\partial \tau} h_a + \bar{m}_a \frac{\partial h_a}{\partial \tau} + m_s \frac{\partial h_s}{\partial \tau} = \\
&= \frac{D_M}{\mu_P} 4\pi R_p^2 \varepsilon \frac{\partial c}{\partial R}\bigg|_{R=R_p} \left[c_{pa}\left(T - 273{,}15\right)\right] + \\
&+ \frac{4}{3}\pi R_p^3 \bar{x} c_{pa} \frac{\partial T}{\partial \tau} + \frac{4}{3}\pi R_p^3 \rho_s c_{ps} \frac{\partial T}{\partial \tau}
\end{aligned} \tag{13}$$

The final form of the energy balance equation is:

$$\begin{aligned}
&\frac{4}{3}\pi R_p^3 \rho_s \left(c_{ps} + \bar{x} c_{pa}\right) \frac{\partial T}{\partial \tau} = \\
&= \frac{D_M}{\mu_P} 4\pi R_p^2 \varepsilon \frac{\partial c}{\partial R}\bigg|_{R=R_p} \left[h_{gl} + h_B - c_{pg}\left(T - T_b\right)\right] - \\
&- 4\pi R_p^2 h_c \left(T - T_b\right)
\end{aligned} \tag{14}$$

The initial and boundary conditions are:

$$\begin{aligned}
&\tau = 0, 0 \le R \le R_p : x = x_i, T = T_i \\
&\tau > 0, \\
&R = 0 : \frac{\partial c}{\partial R}\bigg|_{R=0} = 0 \\
&R = R_p : 4\pi R_p^2 h_m \left(c_b - c\big|_{R=R_p}\right) = \frac{D_M}{\mu_p} 4\pi R_p^2 \varepsilon \frac{\partial c}{\partial R}\bigg|_{R=R_p}
\end{aligned} \tag{15}$$

For a greater accuracy of the results, the

components of the heat of adsorption, respectively latent heat of vaporization and formation enthalpy, are used through actual values (h_{lg} = $f(T)$ and $h_B = f(\overline{x})$). Also, the convection heat transfer coefficient h_c and the mass transfer coefficient h_m on the external surface of the pellet were calculated step by step using the Gnielinski's relations corresponding to the actual parameters.

To solve the balance equations, Crank Nicholson scheme coupled with Gauss elimination algorithm and Euler-Heun finite difference scheme were applied.

3. NUMERICAL RESULTS

For couple silica gel – humid air, characterized by decisive macropore diffusion, adsorption and desorption operations for the following process parameters were studied:

- adsorption T_b=27 °C; y_b=12 g/kg; T_i=80 °C; x_i=22,1 g/kg;
- desorption T_b=127 °C; y_b=6 g/kg; T_i=27 °C; x_i=200 g/kg;
- w_b=0,2 m/s; R_p=3 mm; d_p=88·10^{-9} m.

The numerical results allowed to obtain the evolution of average pellet parameters (Fig. 4, Fig. 6) - water content and temperature – and the water content distribution on radial direction at different times, during adsorption and desorption stages (Fig. 3, Fig. 5).

3.1. Adsorption stage

For the selected conditions the process begins with an extended desorption in the entire pellet (fig. 3); as the contact time between the two phases (air and desiccant solid) increases, desorption is restricted to the center of the pellet; the desiccant solid cools and recovers it's adsorptive properties (Fig. 3, Fig. 4 a); initial desorption is not highlighted in the evolution of $\overline{x}$, apparently the whole pellet being in adsorption phase (differential layers involve with different weights in average water content calculation because of the different volume included);

The average water content of the solid desiccant increases in time, but the process dynamics decreases in time (fig.4 b). The temperature of the pellet decreases quickly in the first minutes because of the intense heat exchange through convection mode on the exterior surface of the pellet and the endothermic effect of the initial desorption in the superficial layers (Fig. 4 a).

Later it can be noticed a linear variation of temperature and uniformity of the gradient $\frac{\partial x}{\partial R}$ within the pellet.

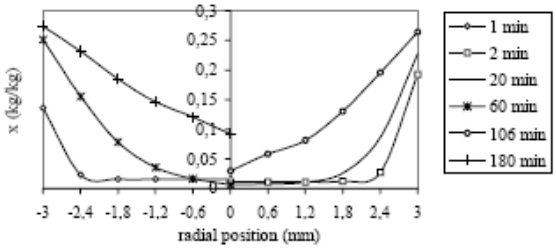

Fig. 3. The water content distribution within the pellet - adsorption operation

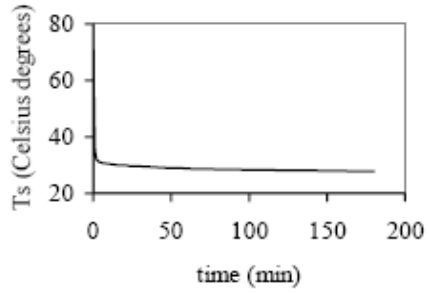

(a)

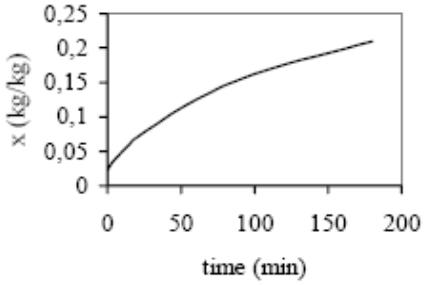

(b)

Fig. 4. The evolution of the average pellet parameters – adsorption operation

3.2. Desorption stage

In desorption stage, the phenomenon are complementary to those presented previously. In figure 5 and 6 b is highlighted the initial adsorption (the average water content raises over the initial level). In the same time the desiccant temperature increases quickly because of the intense convective heat exchange with the warm fluid and due to the released heat of adsorption.

Then, the average water content decreases fast, the successive layers being regenerated. The superficial layers are regenerated relatively quickly but, in the profoundness of the pellet the desorbed vapor move with difficulty because of the small diffusion coefficient D_M (Fig. 5).

The last phase corresponds to the evolution towards the equilibrium state. In fact, the regeneration is made until a residual load about 20 g/kg. Finally, can be noticed that the desorption is faster than adsorption (at least in terms of selected regenerations conditions)

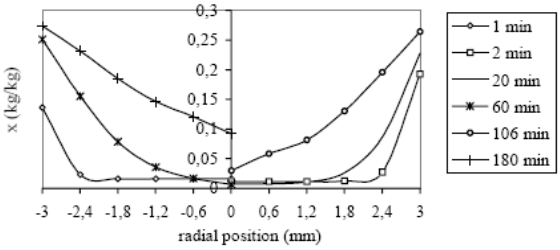

Fig. 5. The water content distribution within the pellet – desorption operation

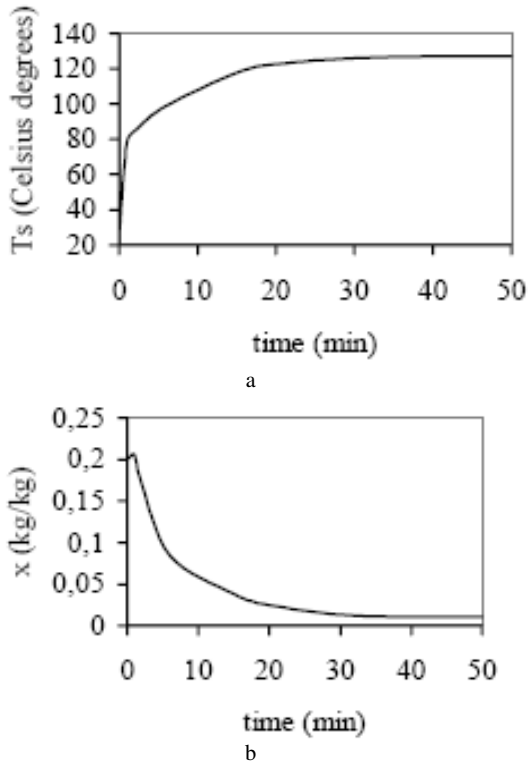

Fig. 6. The evolution of the average pellet parameters-desorption operation

4. CONCLUSIONS

The evolutions of the local and average parameters of the adsorbent pellet reveal the dynamics of the transfer processes and offer valuable information concerning the optimization possibilities of sorption operation. Thus, the model can be used to study the role of the particle size and of the desiccant material type.The work presented in this paper represents the second stage of a theoretical approach of the heat and mass transfer processes which occur within the packed bed adsorbers in fixed or rotary alternatives. In the first stage, a method for numerical simulation of the adsorber operation, based on the assumption of homogeneous pellet parameters, was proposed [7].

The authors plan to develop an integrated model for evaluation the adsorber performances beginning with the transfer processes at the particle level. Thus, the profoundness of the theoretical analysis and the accuracy of the numerical results will increase significantly.

REFERENCES

[1] C. Balaras, G. Grossman, et al. – *Solar air conditioning in Europe-an overview*. Renewable and Sustainable Energy Reviews, 11, 299-314, (2007).

[2] P. Stabat, D. Markio – *Heat and mass transfers modelled for rotary desiccant dehumidifiers*. Applied Energy, 85, 128-142, (2008).

[3] D. La, Y.J. Dai, Y. Li, R.Z. Wang, T.S. Ge –*Technical development of rotary desiccant dehumidification and air conditioning*. Renewable and Sustainable Energy Reviews, 14, 130-174, (2010).

[4] W.W. Kanoldt – *Nicht-isotherme Adsorption am Adsorbenseinzelnkorn*. Dissertation, Tech. Univ. Munchen, (1992).

[5] A. Brunosvska, J. Ilavsky, V. Hlavacek –*An analysis of a nonisothermal one-component sorption in a single adsorbent layer-a simplified model*. Chemical Engineering Science, vol. 36, 123-128, Pergamon Press (1981).

[6] C.E Panaite – *Possibilities of optimization of the adsorption systems utilizing solar energy for air conditioning purposes* "Gheorghe Asachi" Technical University of Iasi, Thesis, (2000).

[7] C.E Panaite, et al – *Experimental Data and Numerical Results on an Advanced Air Conditioning Systems*. Proceedings of ECOS 2002 Conference, Berlin, Germany, 988-994, (2002)

THERMODYNAMIQUE DES SYSTEMES EN CASCADE: ETAT DE L'ART

Michel FEIDT

LABORATOIRE D'ÉNERGETIQUE ET DE MECANIQUE THEORIQUE ET APPLIQUEE (LEMTA), France

Résumé : L'Utilisation Rationnelle de l'ENERGIE a connu plusieurs rebondissements depuis les crises pétrolières des années 1980. Le problème Energétique est devenu, depuis lors, un problème majeur de l'Humanité. Les aspects mis en jeu sont bien sûr Economiques, Environnementaux, mais aussi Scientifiques et Techniques, et alors la Thermodynamique est OUTIL privilégié.
Nous proposons dans cette conférence invitée de faire un état de l'art des systèmes énergétiques en cascade. Si ces systèmes sont connus et modélisés depuis longtemps du point de vue de la Thermodynamique de l'Equilibre, très classique, il n'en pas de même de l'Approche véritablement Thermodynamique, qui a vu le jour en 1957 sous l'impulsion de P. CHAMBADAL et I. NOVIKOV, mais plus fortement seulement depuis 1975 avec l'article de CURZON et AHLBORN.
Un premier paragraphe sera consacré aux cascades de machines à cycles inverses, utilisées tant pour la production de froid que de chaud, voire des effets couplés (chaud et froid : thermofrigopompe).
Des travaux communs avec l'UPB seront référencés à cette occasion (thèse en cours de H. POP).
Dans un second paragraphe seront rapportées les cascades motrices, dont la plus connue, et sans doute la première expérimentée techniquement, est la cascade Turbine à Combustion – Turbine à Vapeur. Mais d'autres cascades existent et ont été étudiées récemment (thèse de M. RADULESCU au LEMTA, UHP Nancy), ou sont en cours d'étude :
- thèse de C. GAY commune UHP Nancy – UT Belfort, sur une cascade Pile a Combustible – moteur de STIRLING
- thèse de B. CULLEN (UT Dublin, Irlande) avec le concours de l'UPB Bucarest et l'UHP Nancy : cascade moteur de OTTO – moteur de STIRLING.
Une tentative de catalogue sera élaborée et proposée à partir de cet examen pour les moteurs ; une comparaison des principales variantes selon les critères thermodynamiques classiques (rendement au sens du premier principe) sera abordée, e les conséquences proposées.
Le dernier paragraphe tentera d'ouvrir le débat et la recherche vers d'autres critères (entropique ; exergétique ; économique ; environnementaux) : d'autres perspectives pourront être évoquées.
Mots-clés : cycles combinés, Thermodynamique en Dimension Finies TDF, Optimisation et simulation de systèmes

Rezumat : Utilizarea Raţională a Energiei a cunoscut multe întorsături ca urmare a crizelor petroliere din anii 1980. Problema Energetică a devenit, astfel, o problemă majoră a umanităţii. Aspectele discutate sunt desigur economice, probleme de mediu, dar şi ştiinţifice şi tehnice, astfel termodinamica devenind un instrument privilegiat.
În aceast articol este propusă analiza în profunzime a sistemelor energetice în cicluri combinate. Dacă aceste sisteme sunt cunoscute şi modelate de mult timp din punct de vedere al termodinamicii de echilibru, foarte clasic, această metodă nu este o abordare întradevăr termodinamică, ce a apărut în 1957 la impulsul lui P. CHAMBADAL şi I. NOVIKOV, dar mult mai puternic după anul 1975 cu articolul lui CURZON şi AHLBORN.
O primă porţiune va fi dedicată cascadelor maşinilor în cicluri inverse, utilizate atât pentru producerea de frig cât şi pentru producerea căldurii, chiar şi efecte combinate (caldură şi frig: termofrigopompe).
Cu această ocazie se face referire la lucrul în comun cu UPB (teza in curs a lui H. POP).
Într-o a doua porţiune sunt prezentate motoare in cicluri combinate, cea mai cunoscută, şi fără îndoială cel mai analizat din punct de vedere tehnic, este ciclul Turbină cu Gaze – Turbina cu Aburi. Dar există şi alte cicluri combinate care au fost studiate recent (teza lui M. RADULESCU la LEMTA, UHP Nancy), sau sunt luate în considerare:
- teza lui C. GAY făcută în cotutelă la UHP Nancy – UT Belfort, despre un ciclu combinat Pilă de Combustie – motor STIRLING
- teza lui B. CULLEN (UT Dublin, Irlanda) cu asistenţa UPB Bucureşti şi UHP Nancy: un ciclu combinat mototr OTTO – motor Stirling.

A fost elaborată şi propusă o metodă de catalogare cu această ocazie a motoarelor; a fost abordată o comparaţie a variantelor principale în conformitate cu criteriile termodinamicii clasice (randament în semnificaţia primului principiu), şi au fost propuse consecinţele.
În ultima parte se încearcă o deschidere a dezbaterii înspre alte criterii (entropice, exergetice, economice, de mediu): putând fi discutate alte perspective.
Cuvinte cheie: cicluri combinate, Termodinamica cu Dimensiuni Finite TDF, Optimizarea si simularea sistemelor.

1. INTRODUCTION

La raréfaction des énergies de type stock (énergies primaires de type pétrole, gaz naturel, charbon, nucléaire), de même que la protection de l'environnement amène à reconsidérer la conception des systèmes de production d'énergies en vue d'une meilleure utilisation des diverses formes d'énergies mises en jeu. Ceci passe par une meilleure intégration fonctionnelle des composants de système à la conception, mais aussi par un meilleur contrôle commande de ceux-ci. La communauté européenne entend à brève échéance, - réduire de 20% les émissions de CO_2 équivalent (diminution de l'effet de serre), - améliorer de 20% l'efficacité énergétique des systèmes et procédés énergétiques – augmenter de 20% la part des énergies renouvelables ou de types flux (essentiellement solaire et biomasse).

Pour ce faire une première voie d'action consiste à développer l'usage de la cogénération chaude [1], qui est une technique bien connue, visant pour l'essentiel à la valorisation thermique des rejets de chaleur de moteurs thermiques quels qu'ils soient. La référence [1] rapporte d'une comparaison de divers moteurs utilisés en cogénération chaude et des bornes supérieures d'énergie récupérable.

L'intérêt de l'analyse exergétique et des critères associés ressort de cette communication. Il est aussi noté des prolongements possibles à développer de façon urgente, à savoir la cogénération froide, voire la trigénération, domaine encore insuffisamment exploré et développé [2].

Une seconde voie d'action consiste à développer l'usage de cycles en cascade, ou combinés. Cette voie n'est pas nouvelle puisque dès les années 1990, l'intérêt des centrales électriques à cycles combinés avait retenu l'attention [3,4]. L. Langston montrait alors que compte tenu des savoir-faire de l'époque (rendement thermique du cycle de Brayton-Joule η_B=*0,40* ; rendement du cycle de Rankine η_R=*0,30*), le rendement thermique du cycle combine η_{CC} valait :

$$\eta_{CC} = \eta_B + \eta_R - \eta_B \cdot \eta_R \qquad (1)$$

Numériquement, on trouve η_{CC}=*0,58*, bien supérieur au rendement de chaque moteur séparé, mais représentant simplement une limite supérieure au rendement du cycle combiné, au sens du premier principe de la Thermodynamique.

Les valeurs pratiques observées à la même époque étaient de 0,52 à 0,54, à cause des irréversibilités de transfert de chaleur intermédiaires et des irréversibilités thermiques et mécaniques en conduites.

Nous proposons ici de reconsidérer la combinaison d'une machine de Brayton avec une machine de Rankine (ou Carnot), mais selon une approche Thermodynamique en Dimensions Finies.

On remarquera que depuis les années 1990, la combinaison des cycles de Brayton-Joule et Rankine a été reconsidérée sous la forme de cycles mixtes (ou autocombinés) par A. Lazzaretto et G. Manente [5]. Les travaux récents de ces deux auteurs montrent comment faire évoluer le cycle simple de Brayton, vers un système plus complexe et efficace d'un point de vue thermodynamique, sur la base de cycles élémentaires.

Les auteurs suggèrent deux étapes successives :

a) L'identification des puits de chaleur du cycle de base, en vue de leur utilisation comme sources de chaleur de la structure évoluée.

b) L'ajout d'autres puits ou sources visant à l'amélioration des performances et/ou efficacité du système amélioré.

L'application de la méthode a été faite sur le cycle de Brayton avec le gaz naturel comme combustible ; l'évolution vers les cycles mixtes (ou autocombinés) est illustrée pour montrer les combinaisons diverses des cycles à gaz et vapeur, de façon très immédiate, mais aussi le développement de cycle de Brayton à oxycombustion avec captage de CO_2, vers le cycles de Graz, S-Graz et H_2/O_2 autocombinés.

La présente communication vise au contraire à une comparaison des diverses combinaisons de cycles possibles particulièrement les cycles à source de chaleur externe (ou combustion externe) dit Moteurs à Combustion Externe (MCE) à savoir les machines de Carnot, Ericsson, Stirling et les Moteurs

à Combustion Interne (MCI) à savoir les machines de Brayton-Joule, Diesel, Otto-Beau de Rochas.

Le paragraphe 2 détaillera le modèle de cascade de référence selon la Thermodynamique en Dimensions Finies, la cascade de Carnot-Carnot.

Le paragraphe 3 présentera le modèle générique de la cascade MCI-MCE, selon l'approche Thermodynamique en Dimension Finies (TDF) ; la particularisation aux trois MCI courants cités sera faite.

Le paragraphe 4 discutera des principaux résultats des modèles et leurs comparaisons, selon diverses contraintes possibles dont l'énergie thermique disponible à la source chaude du système, ou la température maximale de cycles autorisée.

Le paragraphe 5 rapportera des conclusions du présent travail et de ses perspectives.

2. LA CASCADE CARNOT-CARNOT

2.1 Cascade réceptrice

Cette cascade est utilisée de longue date dans le domaine de la réfrigération [6]. De nombreux travaux existent actuellement dans ce domaine, vu l'intérêt pour les fluides frigorigènes dit naturels (NH_3, CO_2, N_2O), et ce pour des applications variées telles que bien sûr le refroidissement à basse température [7] et la congélation [8].

Divers composants sont susceptibles d'être intégrés dans ces cascades [9], dont les compresseurs à 2 vis. Ces mêmes cascades réceptrices peuvent simultanément avoir 2 effets utiles à savoir un effet utile de refroidissement et un effet utile de chauffage [10,11].

Ce point mérite quelques commentaires : nous avons un effet confirmé récemment [12] l'existence d'une température optimale (et conséquemment une pression) selon un modèle TDF pour la machine à froid en cascade.

Il y correspond aussi une répartition optimale des conductances de transfert conformément à ce qui a été montré antérieurement pour une thermofrigopompe à compression mécanique de vapeur simple ; l'optimisation au sens du premier principe a conduit aux conductances thermiques froide K_F* et chaude K_C* optimales suivantes :

$$K_F^* = \frac{1}{2}\cdot\left(K_T - \frac{\dot{S}_i}{\alpha^*}\right) = \frac{\sqrt{K_T}}{2}\cdot\left(\sqrt{K_T} - \sqrt{\dot{S}_i}\right) \quad (2)$$

$$K_C^* = \frac{1}{2}\cdot\left(K_T + \frac{\dot{S}_i}{\alpha^*}\right) = \frac{\sqrt{K_T}}{2}\cdot\left(\sqrt{K_T} + \sqrt{\dot{S}_i}\right) \quad (3)$$

avec

K_T, conductance totale de transfert thermique à distribuer, $\dot{S}_i$, flux d'entropie irréversible créé dans la machine en régime dynamique stationnaire

$$\alpha^* = \sqrt{\frac{\dot{S}_i}{K_T}}$$

Les pincements aux échangeurs à l'optimum d'efficacité sont :

$$X_F^* = T_{SF} - T_F^* = \frac{\alpha^*\cdot T_{SF}}{1+\alpha^*} \quad (4)$$

$$X_C^* = T_{SC} - T_C^* = \frac{\alpha^*\cdot T_{SC}}{1-\alpha^*} \quad (5)$$

T_{SF}, T_{SC}, températures respectives du thermostat froid et chaud.

It y correspond le *COP*, Coefficient de performance de la Thermofrigopompe (TFP) au sens du premier principe $COP^*_{I\,TFP}$.

$$COP^*_{ITFP} = \frac{\left(1+\sqrt{\frac{\dot{S}_i}{K_T}}\right)^2\cdot T_{SC} + \left(1-\sqrt{\frac{\dot{S}_i}{K_T}}\right)^2\cdot T_{SF}}{\left(1+\sqrt{\frac{\dot{S}_i}{K_T}}\right)^2\cdot T_{SC} - \left(1-\sqrt{\frac{\dot{S}_i}{K_T}}\right)^2\cdot T_{SF}} \quad (6)$$

Ce travail a été repris et complété récemment [13] ; la présentation qui en a été faite au colloque SRT de Brasov a montré comment évoluent les conductances optimales en fonction de la charge frigorifique (Figure 1), les pincements optimaux aux échangeurs (Figure 2), puis le COP maximum associé (Figure 3).

Il en résulte un COP optimum-optimorum.

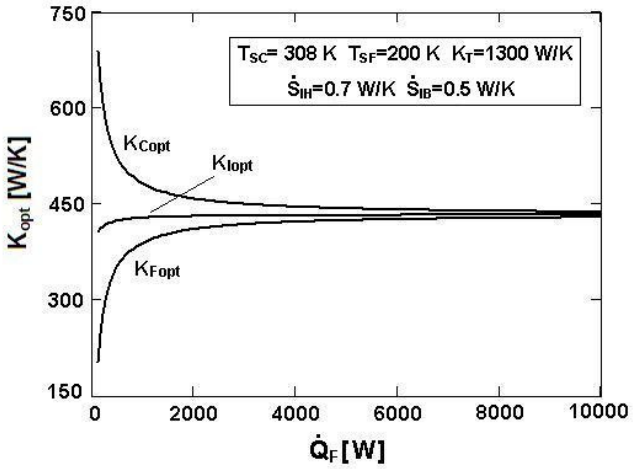

Fig. 1. Conductance optimale en fonction de la charge frigorifique

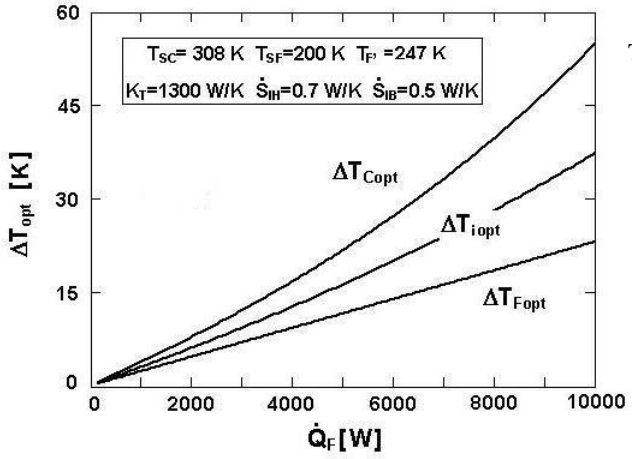

Fig. 2. Les pincements optimaux aux échangeurs

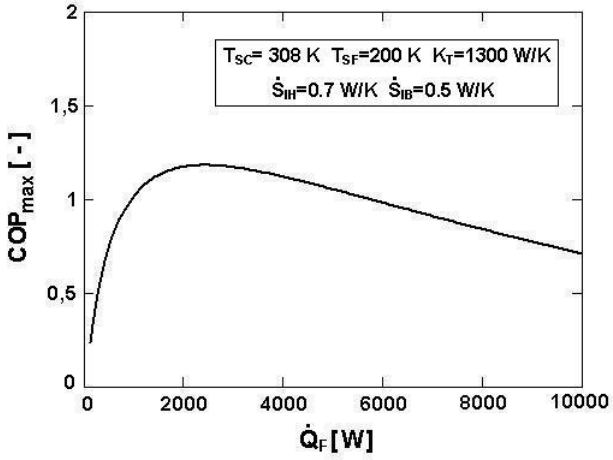

Fig. 3. Le COP maximum associé

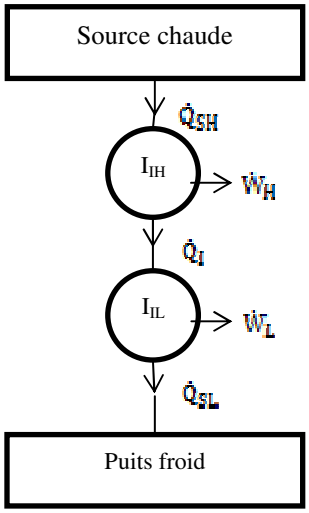

Fig. 4. Représentation schématique de deux moteurs thermomécaniques en cascade

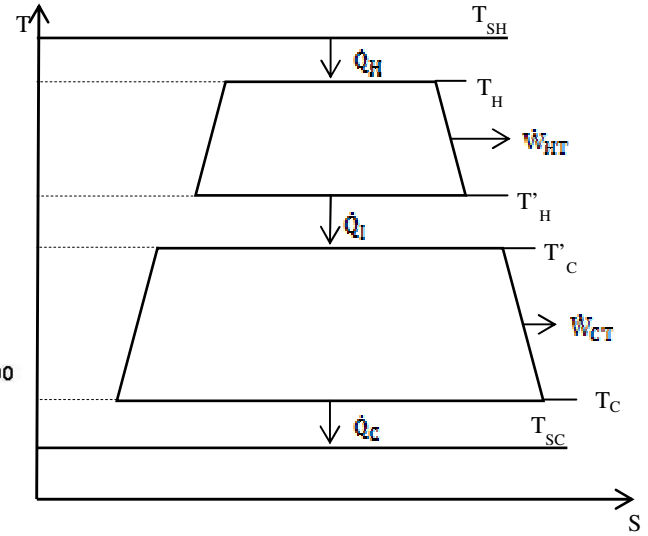

Fig. 5. Diagramme T, S d'une cascade de machines de Carnot adiabatiques, irréversible selon la TDF

2.2 Cascade motrice

Ces travaux se poursuivent dans le cadre d'un travail commun avec G. POPESCU et H. POP (thèse en cours [14]).

A cette approche courante en cascade de cycles récepteurs, correspond l'approche en cycles moteurs dont la publication [15] donne un exemple dans le cas de la récupération d'énergie froide du gaz naturel liquéfié (GNL). Ce travail considère l'efficacité énergétique et exergétique d'un cycle en cascade. Le puits froid est ici associé à la vaporisation du GNL, bien en dessous de la température de l'ambiance.

La cascade analysée comporte trois cycles : le cycle GNL ouvert, le cycle de Brayton-Joule à

combustion de gaz et le cycle de Rankine à mélange NH_3–H_2O.

Il est proposé ci-après de considérer la cascade de cycle de Carnot selon la Thermodynamique en dimensions finies. Cette approche reste complémentaire de celle proposée dans le travail de V. CENUSA [16].

Quelque soit la cascade le système des 2 moteurs thermomécaniques se présente comme un système en série du point de vue de la chaleur transmise, et en parallèle pour la production d'énergie mécanique (ou électrique) : Figure 4.

Le diagramme (T, S) de la cascade sans perte thermique (adiabaticité) mais avec des irréversibilités internes et au contact avec les sources et puis de chaleur est représenté sur la Figure 5.

La Figure 5 montre les deux cycles irréversibles de Carnot, l'un en haute température HT, le second en basse température CT. On remarque sur le diagramme que la source chaude à T_{SH}, comme le puits froid à T_{SC} sont supposés des thermostats.

En régime dynamique stationnaire, les équations du modèle sont fournies par les bilans énergétiques de puissance motrice :

machine HT $$\dot{W}_{HT} = -\dot{Q}_H - \dot{Q}_I \quad (7)$$

machine BT $$\dot{W}_{BT} = -\dot{Q}_I - \dot{Q}_C \quad (8)$$

système $$\dot{W}_T = -\dot{Q}_H - \dot{Q}_C \quad (9)$$

Les bilans entropiques correspondants s'écrivant :

machine HT $$\frac{\dot{Q}_H}{T_H} + \frac{\dot{Q}_I}{T'_H} + \dot{S}_{IH} = 0 \quad (10)$$

machine BT $$\frac{\dot{Q}_C}{T_C} + \frac{\dot{Q}_I}{T'_C} + \dot{S}_{IC} = 0 \quad (11)$$

avec $$\dot{S}_{IH} + \dot{S}_{IC} = \dot{S}_I \quad (12)$$

Les paramètres du problème sont T_{SH}, T_{SC}, K_H, K_C, K_I, $\dot{S}_{IH}$, $\dot{S}_{IC}$, tandis que les variables sont T_H, T_C, T'_H, T'_C. Les conductances de transfert thermique correspondent dans le cas présent à une loi de transfert linéaire conformément à :

$$\dot{Q}_H = K_H \cdot (T_{SH} - T_H) \quad (13)$$

$$\dot{Q}_I = K_I \cdot (T'_C - T'_K) \quad (14)$$

$$\dot{Q}_C = K_C \cdot (T_{SC} - T_C) \quad (15)$$

On suppose par ailleurs une dimension finie de la machine à travers la contrainte supplémentaire :

$$K_H + K_I + K_C = K_T \quad (16)$$

Si de plus on impose $\dot{Q}_H = \dot{Q}_0$ (flux d'énergie disponible imposé), on peut après quelques calculs trouver l'expression du rendement de la cascade sous la forme [17] :

$$\eta_{IM} = 1 - \frac{T_{SC}}{\dot{Q}_0} \cdot \left[\frac{\dot{S}_{IB} \cdot \left(\frac{1}{B} - \frac{1}{K_I}\right) + 1}{\frac{1}{B} - \frac{1}{K_I} - \frac{1}{K_C} - \frac{\dot{S}_{IB}}{K_C} \cdot \left(\frac{1}{B} - \frac{1}{K_I}\right)} \right] \quad (17)$$

avec $$B = \frac{\dot{Q}_0}{T_{SH} - \frac{\dot{Q}_0}{K_H}} + \dot{S}_{IH}$$

Le crochet est une fonction F, des trois conductances K_H, K_C, K_I. Il existe une répartition optimale de ces conductances, facile à trouver, conduisant à un rendement maximum:

$$MAX_{(\eta_{IM})} = 1 - \frac{T_{SC}}{T_{SH}} \cdot \left[\frac{K_T + 2\cdot\dot{S}_I + \frac{1}{C}\left[\dot{S}_I \cdot (K_T + \dot{S}_{IB} - 3\cdot C) + \dot{S}_{IB} \cdot (\dot{S}_{IB} - 3\cdot C - 2\cdot\dot{S}_I)\right]}{K_T + 2\cdot\dot{S}_{IB} - 9\cdot C - 4\cdot\dot{S}_I} \right] \quad (18)$$

avec

$$K_{H_{opt}} = \frac{K_T + 2\cdot\dot{S}_I}{3 + \frac{2\cdot\dot{S}_I - \dot{S}_{IB}}{C}} \; ; \; C = \frac{\dot{Q}_0}{T_{SH}}$$

$$K_{I_{opt}} = K_{H_{opt}} \cdot \frac{B}{A} \; ; \; A = \frac{\dot{Q}_0}{T_{SH} - \frac{\dot{Q}_0}{K_{H_{opt}}}}$$

$$K_{C_{opt}} = K_T - K_{H_{opt}} \cdot \left(1 + \frac{B}{A}\right) \; ; \; B = A + \dot{S}_{IH}$$

Il est à remarquer, que le cas limite endoreversible $(\dot{S}_{IB} = \dot{S}_{IH} = 0)$, restitue l'équipartition des conductances de transfert.

La Figure 6 présente l'évolution du rendement en fonction de $t_{sh} = \frac{T_{SH}}{T_{SC}}$, pour $\dot{q}_0 = \frac{\dot{Q}_0}{K_T \cdot T_{SC}}$ donné et diverses valeurs des paramètres entropiques $\dot{s}_{IB} = \frac{\dot{S}_{IB}}{K_T}$, $\dot{s}_I = \frac{\dot{S}_I}{K_T}$.

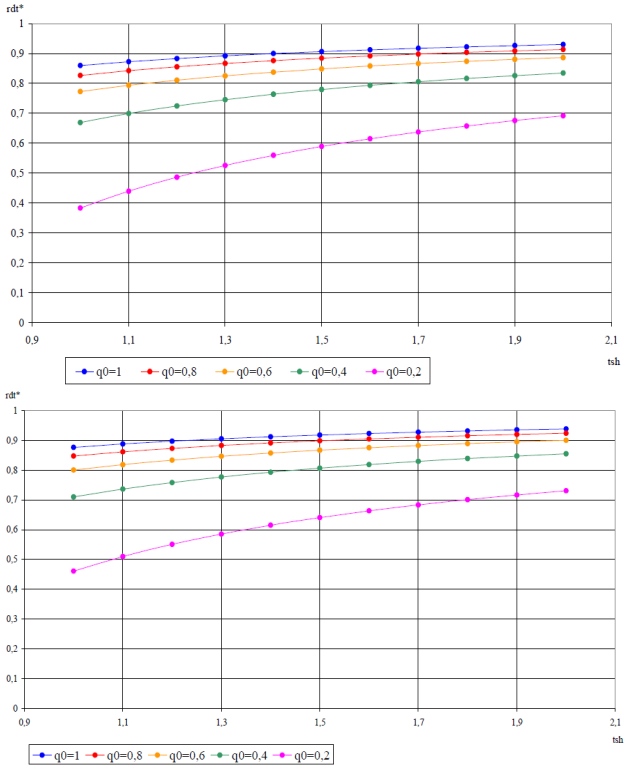

Fig. 6. Evolution du rendement en fonction de la température

On observe une croissance monotone du rendement optimal avec la température de source chaude et une forte influence des irréversibilités sur le rendement.

Une extension du modèle et optimisation pour N cycles ORC en cascade a été proposée récemment [18] dans le cas endoréversible précèdent ; on trouve dans ce cas que :

$$K_{i_{opt}} = \frac{K_T}{N+1} \quad \forall i \tag{19}$$

et $$MAX_{(\eta IM)} = 1 - \frac{T_{SC}}{T_{SH} - \frac{\dot{Q}_0}{K_T}\cdot(N+1)^2} \tag{20}$$

Dans tous les cas rapportés, le $MAX_{(\eta IM)}$ correspond au maximum de puissance délivrée par la cascade.

2.3 Extension aux cascades Carnot-Stirling er Carnot-Ericsson

Cette extension est immédiate, en conservant les mêmes conditions que celles utilisées dans le paragraphe 2.2, à savoir pas de pertes thermiques, endoréversibilité et lois de transfert linéaires.

La Figure 7 présente les cycles associés à la cascade de Carnot-Stirling ; il faut simplement préciser que le résultat est identique à celui de la cascade Carnot-Carnot en régénération totale. Il en est de même pour la cascade Carnot-Ericsson en récupération totale cette fois. Les bornes obtenues sont donc les bornes supérieures des maximum de rendement ou de puissance a $\dot{Q}_0$, fourniture de chaleur disponible connue.

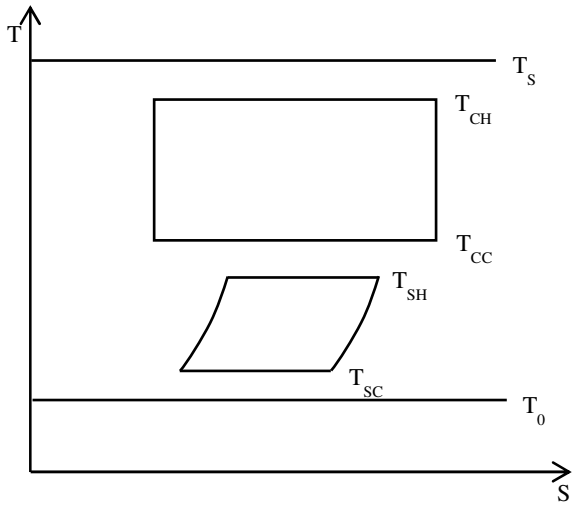

Fig. 7. Cycles de la cascade Carnot–Stirling

3. CASCADE MOTEUR A COMBUSTION INTERNE – MOTEUR A COMBUSTION EXTERNE

3.1 Cycles combinés

La cascade la plus courante est utilisée pour les fortes puissances sous forme de ce qui est appelé les cycles combinés (IGCC en anglais). Un cycle combiné associe une turbine à combustion TAC à une turbine à vapeur (d'eau) TV, valorisant la chaleur disponible sur les fumées. Le couplage porte donc sur un moteur à combustion interne à flux (cycle de Joule-Brayton) avec un moteur à combustion externe de Carnot dans le principe, de Rankine puis Hirn dans la pratique à travers une chaudière récupérative.

On rapporte ici de l'optimisation d'un cycle combiné, par la méthode des courbes composites CC, visant à minimiser le pincement P et les irréversibilités thermiques du système proportionnelle à l'aire entre les 2 courbes (Fig. 8).

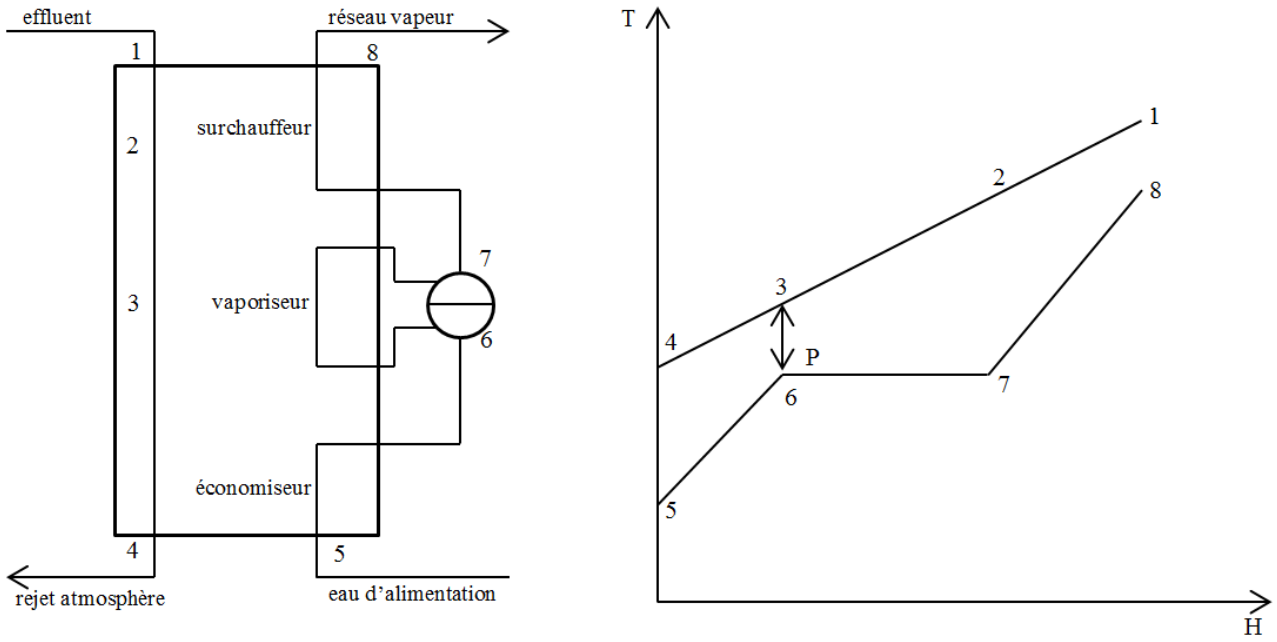

Fig. 8. Courbes composites d'un générateur de vapeur

L'optimisation a été effectuée numériquement en utilisant le logiciel Thermoptim. L'objectif est une production minimale de 430 MW électrique, à partir de 4 configurations : le cycle combiné simple (1P), le cycle combiné à resurchauffe (2P, 2 pressions), le cycle combiné à resurchauffe (3P), le cycle combiné avec 1 soutirage a mélangeage (à la pression intermédiaire choisie en 2P). Les valeurs des paramètres sont données dans le tableau 1. Les résultats de l'optimisation avec contraintes sont rapportés dans le tableau 2.

Tableau 1
Valeurs des paramètres du système

combustible	gaz de Montoir – CH_4 87% ; C_2H_6 9% ; C_3H_8 2,5% ; C_4H_{10} 1% rendement de combustion – η_{comb} = 0,95
TAC	rendement isentropique compresseur – η_{isC} = 0,80 rendement isentropique de turbine - η_{isT} = 0,85 T_{air} = 27°C T_0 entrée turbine, TIT = 1220°C T_1 sortie turbine, TOT = 570°C
chaudière récupérative	T sortie chaudière récupération = 120°C T entrée chaudière récupération = 550°C P, pincement = 20°C
TV	T surchauffe, resurchauffe = 550°C
	T_{eau} = 18°C $T_{condensation}$ = 24°C pincement au condenseur = 6°C $P_{condensation}$ = 30 mbar $P_{maximale}$ = 135 bar rendement isentropique de pompe = 0,80 rendement isentropique de turbine = 0,85 titre en vapeur en sortie turbine > 0,85
Alternateur	rendement électrique – η_{elec} = 0,90

Tableau 2
Résultats de l'optimisation

Cycle Combiné	simple 1P	à resurchauffe 2P	à 2 resurchauffes 3P – 2R	à 1 soustirage (P = 39bar)
Puissance electrique	430 MW	460 MW	471 MW	<430 MW
Pressions		P_{RS1} = 39 bar	P_{RS2} = 4,7 bar	
Rendement	0,527	0,528	0,546	0,498
Pincement	120°C	90°C	50°C	

Ce tableau amène les commentaires du choix de la pression de 39 bars, en présence de resurchauffe : ce choix résulte de compromis entre maximum de rendement (à 51 bars) et puissance. Cette pression est aussi celle retenue pour le soutirage. La fraction optimale du soutirage (0,327) ne permet pas d'atteindre les 430 MW électrique requis, avec les débits d'air (730 kg/s), d'eau (54 kg/s) et de gaz

(14,3 kg/s). La technique de soutirage n'est pas intéressante en cycle combiné.

Enfin quelques calculs complémentaires permettent de trouver que la production de CO_2 par kWh produit passe de 648,9 g/kWh pour la turbine à combustion seule, à 298 g/kWh (soit un rapport de 2,18 très conséquent du point de vue environnemental).

3.2 Cascade TAC-Stirling

La Figure 9 présente les cycles imbriqués de cette cascade, pour laquelle on suppose l'endoréversibilité des cycles (cas limite), aussi qu'un cycle de Joule-Brayton sans récupération et un cycle de Stirling en régénération totale.

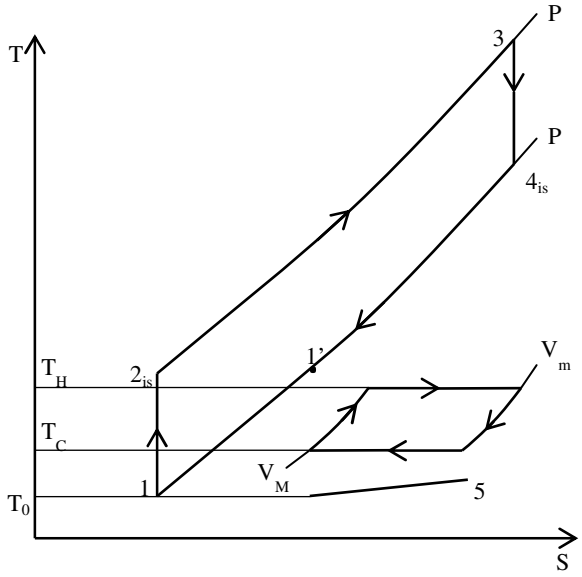

Fig. 9. Représentation des cycles de Brayton-Joule et Stirling en cascade

Il est alors facile de montrer que la puissance mécanique maximale de la TAC vaut :

$$\left|\dot{W}_{TAC}\right| = \dot{C}_T \cdot [(T_3 - T_4) - (T_2 - T_0)] \qquad (21)$$

avec $\dot{C}_T = \dot{M}_T \cdot C_{pT}$ et $\frac{T_0 \cdot T_3}{T_2 \cdot T_4} = 1$ (endoreversibilité)

De meme pour le moteur de STRILING, dont la puissance maximale vaut :

$$\left|\dot{W}_S\right| = \dot{q}_H + \dot{q}_C \qquad (22)$$

avec $\dot{q}_H = \varepsilon_H \cdot \dot{C}_T \cdot (T_4 - T_H)$

$\dot{q}_C = \varepsilon_C \cdot \dot{C}' \cdot (T_0 - T_C)$

$$\frac{\dot{q}_H}{T_H} + \frac{\dot{q}_C}{T_C} = 0$$

$\varepsilon_H, \varepsilon_C$, efficacité des échangeurs chaud et froid de la cascade ; $\dot{C}' = \dot{M}' \cdot C_p'$.

La puissance totale $\left|\dot{W}_{TOT}\right|$ s'en déduit aisément ; elle dépend des variables T_2, T_4, T_H, T_C, des paramètres $\dot{C}_T, \dot{C}', \varepsilon_H, \varepsilon_C$. A des fins de comparaison nous imposons la dépense énergétique de la cascade $\dot{q}_0 = \dot{C}_T \cdot (T_3 - T_2)$ et la température maximale associée $T_3 = T_{MAX}$. Compte tenu des 2 contraintes d'endoreversibilité, il subsiste un degré de liberté. L'optimisation en température conduit alors, après calcul analytique à :

$$T_C^* = \sqrt{T_0} \cdot \frac{\varepsilon_H \cdot \dot{C}_T \cdot \sqrt{T_4^*} + \varepsilon_C \cdot \dot{C}' \cdot \sqrt{T_0}}{\varepsilon_H \cdot \dot{C}_T + \varepsilon_C \dot{C}'} \qquad (23)$$

$$T_H^* = \sqrt{T_4} \cdot \frac{\varepsilon_H \cdot \dot{C}_T \cdot \sqrt{T_4^*} + \varepsilon_C \cdot \dot{C}' \cdot \sqrt{T_0}}{\varepsilon_H \cdot \dot{C}_T + \varepsilon_C \cdot \dot{C}'} \qquad (24)$$

$$T_4 = T_0 \cdot \left[\frac{A}{A - \frac{\dot{q}_0}{T_{MAX}}}\right]^4 \qquad (25)$$

avec $T_2 = T_{MAX} - \frac{\dot{q}_0}{\dot{C}_T}$; $A = \frac{\varepsilon_H \cdot \dot{C}_T \cdot \varepsilon_C \dot{C}'}{\varepsilon_H \cdot \dot{C}_T + \varepsilon_C \cdot \dot{C}'}$

Il y correspond, la puissance optimale de la cascade $\left|\dot{W}_{TOT}\right|^*$:

$$\left|\dot{W}_{TOT}\right|^* = \dot{q}_0 \cdot \left(1 - \frac{T_0}{T_{MAX}} \cdot \frac{1}{1 - \frac{\dot{q}_0}{A \cdot T_{MAX}}}\right) \qquad (26)$$

On voit alors qu'à $\dot{C}_T, \dot{C}'$ paramètres, mais efficacités d'échangeurs variables mais finies (à travers les dimensions géométriques : surfaces) selon : $\varepsilon_H + \varepsilon_C = \varepsilon_T \leq 2$, il existe un maximum pour $\left|\dot{W}_{TOT}\right|^*$ si A est lui-même maximum ; ceci se produit pour :

$$\varepsilon_H^* = \varepsilon_T \cdot \frac{\sqrt{\dot{C}'}}{\sqrt{\dot{C}_T} + \sqrt{\dot{C}'}} \qquad (27)$$

$$\varepsilon_C^* = \varepsilon_T \cdot \frac{\sqrt{\dot{C}_T}}{\sqrt{\dot{C}_T} + \sqrt{\dot{C}'}} \qquad (28)$$

d'où :

$$MAX\left|\dot{W}_{TOT}\right|^* = \dot{q}_0 \cdot \left(1 - \frac{T_0}{T_{MAX}} \cdot \frac{1}{1 - \frac{\dot{q}_0}{A \cdot T_{MAX}}}\right) \qquad (29)$$

avec $A^* = \varepsilon_T \cdot \frac{\dot{C}_T \cdot \dot{C}'}{\left(\sqrt{\dot{C}_T}+\sqrt{\dot{C}'}\right)^2}$

Les relations (20, 29) permettent une comparaison entre les cascades MCE-MCE puis MCI-MCE à $\dot{q}_0$ et T_{MAX} identiques, dans les conditions optimisées ; ceci est de nature à guider dans les choix de la configuration de système.

On remarquera par ailleurs qu'à T_{MAX} imposé, ainsi que les débits calorifiques à la source $\dot{C}_T$ et puits $\dot{C}'$, il existe une dépense énergétique de cycle optimale $\dot{q}_0^*$, conduisant à un maximum maximorum de $|\dot{W}_{TOT}|^*$:

$$\dot{q}_0{}^* = A^* \cdot \left(\sqrt{T_{MAX}} - \sqrt{T_0}\right) \quad (30)$$

$$MAX[MAX|\dot{W}_{TOT}|^*] = \varepsilon_T \cdot \frac{\dot{C}_T \cdot \dot{C}'}{\dot{C}_T+\dot{C}'} \left(\sqrt{T_{MAX}} - \sqrt{T_0}\right)^2 \quad (31)$$

Ceci conduit à un résultat original et nouveau : les débits calorifiques sont en effet finis tels que $\dot{C}_T + \dot{C}' = \dot{C}$.

Il apparait donc une distribution optimale de ces débits calorifiques conduisant à une quatrième optimisation de la puissance mécanique de la cascade :

$$OPT\{MAX[MAX|\dot{W}_{TOT}|^*]\} = \varepsilon_T \cdot \frac{\dot{C}}{4} \cdot \left(\sqrt{T_{MAX}} - \sqrt{T_0}\right)^2 \quad (32)$$

Cet optimum, en endoreversible est associé à l'équipartition des débits calorifiques :

$$\dot{C}' = \dot{C}_T = \frac{\dot{C}}{2} \quad (33)$$

Le même type de raisonnement s'applique aux cascades moteur de OTTO-Stirling, moteur de Diesel-Stirling, ou de façon général moteur à cycle mixte-Stirling.

La transposition est immediate pour les cascades MACI-Carnot ou MACI-Ericsson (résultats disponibles auprès de l'auteur).

3.3 Cascade moteur de OTTO-Stirling

La démarche de modélisation est strictement identique à celle développée dans le paragraphe précédent et conduit au même genre de résultat. Nous ne reprenons donc pas.

Le présent paragraphe rend plutôt compte de résultats obtenus dans une recherche commune entre notre université (UHP Nancy), l'UPB et l'université de Dublin, à l'occasion de la récente thèse de B. Cullen [20].

Le choix du couplage entre un moteur à combustion interne de OTTO et un moteur à combustion externe de Stirling résulte du fait que ces 2 moteurs sont bien connus ; les applications visées sont tant dans la petite industrie, que le transport ou l'habitat (système distribué de production d'énergie). Des modèles selon la FTT ont été proposés dans [20] pour le moteur de OTTO (chapitre 3) et le moteur de Stirling (chapitre 5) ; la validation en a été faite respectivement aux chapitres 4 et 6. On rapporte ici des principaux résultats obtenus sur la cascade (chapitre 7).

On notera que la prise en compte des irréversibilités se fait par la méthode du ratio ; il en résulte une corrélation I_R pour le moteur de OTTO (Figure 10) en fonction de la vitesse de rotation.

On remarque que pour le moteur de Stirling, la pression de charge du moteur est aussi un paramètre déterminant.

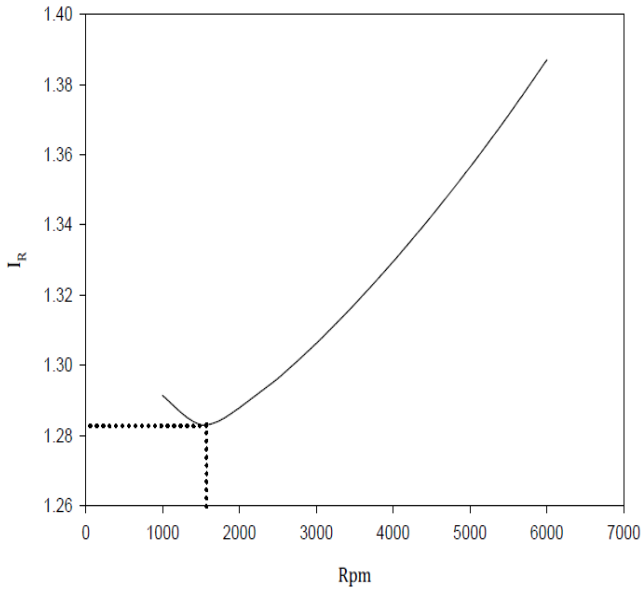

Fig. 10. Parametre d'ireversibilite I_R, pour le moteur OTTO

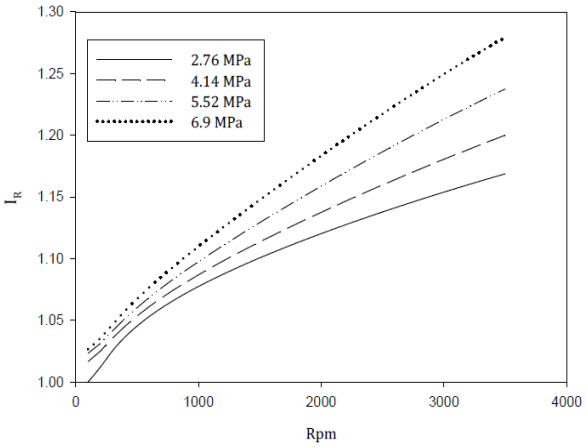

Fig. 11. Parametre d'ireversibilite I_R, pour le moteur Stirling

L'optimisation de la cascade proposée a été réalisée dans un mode synchrone (les 2 moteurs sont à la même vitesse) ou en mode asynchrone (les 2 moteurs sont découplés). La température de sortie des fumées du cycle de OTTO est particulièrement importante pour le modèle, et a été calculée comme une température enthalpique moyenne [20] en régime dynamique stationnaire.

Tableau 3

Performance du cycle combiné, opération synchrone

Performance du cycle Otto				**Valeur**
$P_{combustible}$ (à 1500 rpm) (kW)				21,43
P_{break} (à 1500 rpm) (kW)				6,07
η_{break} (à 1500 rpm) (%)				28,3
Pression moyenne du cycle (MPa)	2,76	4,14	5,52	6.9
Performance du cycle Stirling				
P_{break} (à 1500 rpm) (kW)	0,99	1,82	2,97	-
η_{break} (à P_{max}) (%)	18,6	22,9	27,6	-
Performance du cycle combiné				
P_{break} (kW)	7,06	7,89	9,04	-
$\eta_{CC,break}$ (%)	32,9	36,8	42,2	-
Gain de performance				
P_{break} (à 1500 rpm) (%)	16,3	29,9	48,9	-
η_{break} (%) (absolute)	4,6	8,5	13,9	-
η_{break} (%) (relative)	16,2	30	49,1	-

Les résultats de la simulation en mode synchrone sont donnés dans le Tableau 3 ou apparaissent les divers gains en comptés : selon l'objectif on voit que ces gains sont dans la plage 5% - 50% donc significatif même si la cascade n'est pas à l'optimum ni en puissance, ni en rendement.

La même étude faite en mode asynchrone vise à la maximisation du rendement total, η_{CC}. Ceci apparait sur les courbes de la Figure 12.

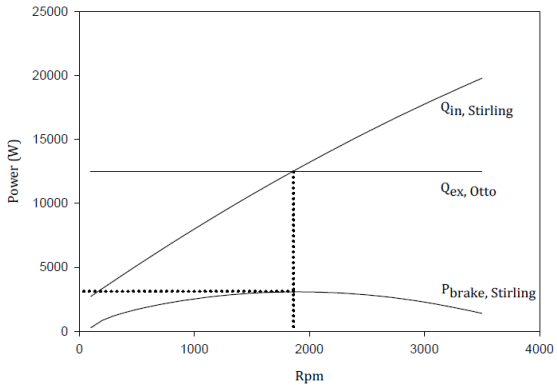

Fig. 12. Opération du GPU-3 en réservoir thermal d'évacuation OTTO

L'ensemble des résultats est rapporté dans le Tableau 4 :

Tableau 4

Performance du cycle combiné, opération asynchrone

Performance du cycle Otto	**Valeur**			
$P_{combustible}$ (à 1500 rpm) (kW)	21,43			
P_{break} (à 1500 rpm) (kW)	6,07			
η_{break} (à 1500 rpm) (%)	28,3			
Pression moyenne du cycle (MPa)	2,76	4,14	5,52	6.90
Performance du cycle Stirling				
P_{break} (à 1500 rpm) (kW)	1,04	1,92	3,08	3,78
η_{break} (à P_{max}) (%)	16,7	20,0	24,3	25,7
Performance du cycle combiné				
P_{break} (kW)	7,11	7,99	9,15	9,85
$\eta_{CC,break}$ (%)	33,2	37,3	42,7	46,0
Vitesse à P_{max} (rpm)	1770	1924	1860	1380
Gain de performance				
P_{break} (à 1500 rpm) (%)	17,1	31,6	50,7	65,6
η_{break} (%) (absolute)	4,9	9,0	14,4	18,6
η_{break} (%) (relative)	17,3	31,8	50,9	65,7

L'étude peut être étendue à l'efficacité au sens du second principe de la Thermodynamique voir le chapitre 7 de la référence [20].

4. CONCLUSIONS – PERSPECTIVES

a) La présente conférence propose une revue de l'état de l'art dans le domaine des cascades ou des cycles combinés. L'intensité des problèmes énergétiques actuels et à venir, vont dans le sens d'une reconsidération des cascades motrices sur la base des moteurs à Combustion Interne et Externe.

Les cascades correspondantes ont été rapportées et examinées selon la Thermodynamique en Dimension Finies ; les optimisations correspondantes montrent l'existence d'optimum-optimorum qui peuvent servir de références pour la qualification des systèmes réels.

b) Une comparaison entre diverses alternatives est aussi possible.On retiendra que pour une cascade MCE-MCE, le maximum maximorum de rendement au sens du premier principe vaut :

$$MAX\,\eta_{ICC} = 1 - \frac{T_{SC}}{T_{SH} - \frac{\varepsilon \cdot \dot{Q}_0}{K_T}} \tag{34}$$

alors que pour une cascade MCI-MCE (les plus courantes) le maximum maximorum correspond vaut :

$$MAX\,\eta_{ICC} = 1 - \frac{T_0}{T_{MAX} - \frac{\varepsilon \cdot \dot{Q}_0}{\dot{C}}} \tag{35}$$

A même $\dot{Q}_0$ disponible et valeurs de K_T, $\dot{C}$ comparable, on en déduit que lorsque $T_{SH} = T_{MAX}$ et $T_{SC} = T_0$, les rendements maximum maximorum sont équivalents et décroissants de $\dot{Q}_0$.

c) D'assez nombreux travaux ont été fait dans le groupe de recherche rendant compte de ces cascades :

- à cycles inverses (travaux avec H. POP)
- turbine à combustion – turbine à vapeur (travaux avec V. CENUSA)
- moteur de OTTO – moteur de Stirling (travaux avec B. CULLEN)

Ils se poursuivent actuellement suite à la thèse de M. RADULESCU (cascade pile à combustible – turbine à combustion), vers des systèmes en cascade moins courants cascade pile à combustible moteur de Stirling (C. GAY).

d) D'autres critères économiques et environnementaux d'évaluation sont en cours d'étude.

REFERENCES

[1] Feidt, M., *"Thermodynamics and optimization of combined heat and power systems: comparison of various systems"*, 23d International Conference on Efficiency, Cost, Optimization, Simulation and Environmental Impact of Energy Systems, Lausanne, Switzerland, 2010

[2] Feidt, M., *"note d'information cogeneration/ trigeneration"*, IIF-IIR, soumise pour publication (7 pages)

[3] Horlock, J.H., *"Combined Power Plant"*, Pergamon Press, 1992

[4] Langston, L., *"Combined Cycle Power Plant"*, Global Gas Turbine News (IGTI), Feb. 1994, p. 24-25

[5] Lazzareto, A., Manente, G., *"Analysis of Superimposed Elementary Thermodynamic Cycles: from the Brayton-Joule to Advanced Mixed (Autocombined) Cycles"*, International Journal of Thermodynamics, vol. 12 (no 3), Sept. 2009, p. 123-130

[6] Feidt, M., *"Thermodynamics and energetic optimization of systems and processes"* (in Romanian), Bren ed., 2001

[7 Dopazo, A., Fernandez-Seara, J., Sieres, J., Uhia, F.J., *"Theoretical analysis of a CO_2-NH_3 cascade refrigeration system for cooling applications at low temperatures"*, Applied Thermal Engineering, 29 (2009), p. 1577-1583

[8] Dopazo, A., Fernandez-Seara, J., *"Experimental evaluation of a cascade refrigeration system prototype with CO_2 and NH_3 for freezing process applications"*, International Journal of Refrigeration, no 34 (2011), p. 257-267

[9] Wang, B., Wu, H., Li, J., Xing, Z., *"Experimental investigation on the performance of NH_3/CO_2 cascade system with twin screw compressor"*, International Journal of Refrigeration, no 31 (2009), p. 1358-1365

[10] Battacharya, S., Garcia, A., Sarkar, J., *"Thermodynamic analysis and optimization of a novel N_2O-CO_2 cascade system for refrigeration and heating"*, International Journal of Refrigeration, no 32 (2009), p. 1077-1084

[11] Byrne, P., Miriel, J., Lenat, Y., *"Design and simulation of a heat pump for simultaneous heating and cooling using HFC or CO_2 as a working fluid"*, International Journal of Refrigeration no 31 (2009), p. 1711-1723

[12] Boussehain, R., Dimitrov, D., Feidt, M., *"Utilisation simultanée de chaleur et de froid en industrie agroalimentaire, à l'aide de machines à compression de vapeur: quell critére d'efficacité?"*, Colloque Francophone sur l'Énergie, Environnement, Économie et Thermodynamique, Iasi, 2010

[13] Pop, H., Feidt, M., Popescu, G., Apostol, V., Alionte, C.G., *"Optimization of conventional irreversible cascade refrigeration systems"*, (communication colloque SRT Brasov), en cours de publication dans UPB Scientific Bulletin (ISSN 1454-2331)

[14] Pop, H., Thèse de doctorat, en cours de préparation, UPB

[15] Lu, T., Wang, K.S., *"Analysis and optimization of a cascading power cycle with liquefied natural gas (LNG) cold energy recovery"*, Applied Thermal Engineering, vol 29 (2009), p. 1478-1484

[16] Cenusa, V., Thèse de doctorat en cotutelle UHP-UPB, 25.10.2004
[17] Carvalho, V., *"Optimisation Energétique: Cascade CARNOT-CARNOT"*, Thèse de Master R.
multiscale geometries, D. Quciros-Conde, M. Feidt
[18] Laheurte, G., Feidt, M., Boussehain, R., Quciros-Conde, D., *"Constructal cascade of Carnot engine cycles",* chapter IX, p. 107-113, in Constructal theory and editeurs, Presses de l'ENSTA, 2010, ISBN 9 782722 509214
[19] Pierotti, L., Haddad, M., *"Optimisation de cycles combinés gaz"*, rapport de projet de fin d'études, ENSEM-INPL, Nancy, Mars 2011
[20] Cullen, B., *"The Combined Otto and Stirling Cycle Prime-Mover based Power Plant"*, PhD Dublin Institute of Technology, 2010